ABSTRACT

Title of Thesis:	An Experimental Study of Heat Transfer Performance Enhancement by Applying Oscillating Flexible Structures
	Beihan Zhao, Master of Science, 2018
Thesis Directed By:	Professor Bao Yang and Professor Xinan Liu Department of Mechanical Engineering

In this thesis, the effects of a flow-induced oscillating flexible structure on the convective heat transfer of a plate heat exchanger in a vertical rectangular wind tunnel were experimentally investigated. A variable speed fan was used to create an air flow with speed ranging from $9\ \mathrm{m/s}$ to $20\ \mathrm{m/s}$. A flexible structure was placed in the front of the plate heat exchanger, which would oscillate in the air flow. Different shapes and dimensions of flexible structures were tested. The temperature of the plate was monitored, and the steady-state temperature was recorded for each experimental condition. The oscillating motions of the flexible structures were captured with a high-speed camera. Compared to the steady flow convection, the use of the oscillation flexible structure can enhance the mixing of the high-temperature boundary flow with the lower temperature flow and disrupt the boundary layer. The length and width of the rectangular structures were found to have large influence on the oscillating characteristics and the convective heat transfer enhancement. Dimensionless

parameters including flow-induced oscillation frequency, f^*, and coverage ratio, A^*, were also studied in order to discover the relationship between them. Experimental results showed that the structures with a rectangular shape can most significantly improve the convective heat transfer among those various shapes used in the present study. The average heat transfer coefficient was improved from $113\ [\mathrm{W/(m^2 * K)}]$ to $161\ [\mathrm{W/(m^2 * K)}]$ when the inlet wind velocity was $17.2\ [\mathrm{m/s}]$, and that specific rectangular structure had a length of $0.075\ [\mathrm{m}]$ and a width of $0.102\ [\mathrm{m}]$.In addition, highest heat transfer performance was found when $0.22 \leq f^* \leq 0.32$, which could be used for possible further design optimizations.

AN EXPERIMENTAL STUDY OF HEAT TRANSFER PERFORMANCE ENHANCEMENT BY APPLYING OSCILLATING FLEXIBLE STRUCTURES

by

Beihan Zhao

Thesis submitted to the Faculty of the Graduate School of the
University of Maryland, College Park, in partial fulfillment
of the requirements for the degree of
Master of Science
2018

Advisory Committee:
Professor Bao Yang, Advisor, Chair
Research Associate Professor Xinan Liu, Co-Advisor, Co-Chair
Associate Professor Amir Riaz
Research Professor Yunho Hwang

Dedication

To My Parents, and All Others that Helped.

Acknowledgements

I would like to thank Dr. Bao Yang, my advisor, for allowing me to join his group two years ago as an M.Eng. student and transition into the M.S. program. He along with Dr. Xinan Liu, my co-advisor, have been essential in the research I have conducted as part of this thesis. They are always willing to help and offered me numerous suggestions that I could benefit for a long time. I am also grateful for their Teaching Assistant nomination, which largely released my financial burden. I am also grateful to have also received assistance from many others including Mr. Majid Aroom, David Kriesberg from the machine shop.

I appreciate the help from professors and staff within the Mechanical Engineering Department, University of Maryland, College Park. Sincere thanks to my Thesis Defense Committee of Dr. Yunho Hwang and Dr. Amir Riaz in addition to Dr. Bao Yang and Dr. Xinan Liu. I was also assisted throughout my research by fellow lab colleagues Chaolun Zheng, Yong Pei, and Wenshuo Yang.

Table of Contents

Dedication ii

Acknowledgements iii

Table of Contents iv

List of Tables vi

List of Figures vii

Nomenclature x

Chapter 1: Introduction 1

1.1 Background 1

Chapter 2: Experimental Setup 10

2.1 Experimental Facilities: 10

2.2.1 Thermal Experimental Setup 13

2.2.2 Dynamic Observation Experimental Setup 18

Chapter 3: Calculation Methods 21

3.1 Calculation Methods 21

Chapter 4: Hotplate Experiments for System Validation 26

Chapter 5: Effects of Different Shapes 33

5.1 Effects of Small Stripes 33

5.2 Effects of Various Shapes 36

Chapter 6: Effects of Dimensional Parameters and Oscillation Frequencies for Rectangular Textiles 44

6.1 Textile Design: 44

6.2 Thermal Experiments 45
6.3 Effect of Oscillating Frequency 49
6.3.1 Stable Oscillation under Different Wind Inlet Velocities 49
6.3.2 Unexpected Dynamic Motions at Irregular Regimes 56
6.4 Dimensionless Analysis 60
Chapter 7: Research Contributions and Conclusions 67
7.1 Research Contributions: 67
7.2 Conclusions: 68
Chapter 8: Recommendations for Future Work 70
Bibliography 72

List of Tables

Table 1 Experimental facilities with its accessories 12

Table 2 Selected experimental conditions 17

Table 3 ΔT gathered from flat plate experiments 26

Table 4 HTC of flat plate experiments 26

Table 5 Comparison of the Nu from Ginelinski correlations and experimental data. 29

Table 6 Temperature differences monitored from simulating results compared to average experimental data..... 30

Table 7 Source of uncertainty and error in CFD simulations 32

Table 8 Oscillating frequency observed through high speed camera (with 6 different wind inlet velocities: from top to bottom small cells: 9.9 m/s; 12.1 m/s; 14.0 m/s; 15.7 m/s; 17.1 m/s; 18.5 m/s)..... 54

Table 9 Flow-induced oscillation frequency calculated for each rectangular dimension(with 6 different wind inlet velocities: From top to bottom small cells: 9.9 m/s; 12.1 m/s; 14.0 m/s; 15.7 m/s; 17.1 m/s; 18.5 m/s)..... 62

List of Figures

Figure 1 Common vortex generators and the associated geometrical definitions (Adapted from reference [18]) 2

Figure 2 Schematic illustration for a semi-dimple vortex generators (Adapted from reference [20]) 3

Figure 3 Schematic illustration of computational domain for FVG simulations by Ali (Dimensions in mm; Adapted from reference [21]) 4

Figure 4 Schematic for piezoelectric fan experiments (Adapted from reference [24].) 5

Figure 5 Schematic rendering of the flow within a channel cooled by a vibrating reed 6

Figure 6 Schematic illustrations of laser-machined reeds with micro-fabricated surface features with micro-fabricated surface features (Adapted from reference [28]) 7

Figure 7 Schematic of experimental setup for (a) heat transfer measurement and (b) dynamics observation of textile flap 10

Figure 8 Desktop 3D printer Folger Tech 2020 i3 14

Figure 9 CAD models designed for the different flexible structure placements 15

Figure 10 Integrated heat transfer area schematic. 16

Figure 11 Pressure drop measurement setup 18

Figure 12 Pressure drop comparison between 1). Hotplate only; 2). 3D printed solid structure added 18

Figure 13 Visualization of experimental platform 19

Figure 14 Vision research PCC software interface 20

Figure 15 HTC performance for hotplate experiments 27

Figure 16 Comparison between $Nuexperimental$ and $NuGnielinski\ Correlation$ 28

Figure 17 ANSYS fluent simulation interface and sample results (from top to bottom): a). Mesh setup (with inflation to indicate boundary layers); b). Sample Simulation Results (Velocity streamline under the situation of velocity inlet of 9.9 m/s); c). Cross surface local pressure rendering 31

Figure 18 Initial Trying of Using Small Self-Oscillating Rectangular Sheets 33

Figure 19 Experimental results of the initial approach on stripe structures 34

Figure 20 Stripes on hotplate schematic 35

Figure 21 Experimental results of the second approach on stripe structures 35

Figure 22 Schematic of different structure shapes 36

Figure 23 HTC experimental results with different shape of flexible structures 38

Figure 24 Most significant enhancement among different shape testing 38

Figure 25 HTC performances with different shapes with fixed At 40

Figure 26 HTC results based on initial dimensional hypothesis 42

Figure 27 HTC performance controlled L (0.14 m) with W in (1) 0.08 m; (3) 0.035 m 43

Figure 28 Schematic of selected shapes of rectangular textiles with meshes 44

Figure 29 Scatter for HTC performance of different dimensions of rectangular structures. Legend in unit: cm 45

Figure 30 HTC in respect of U (Fixed W) 46

Figure 31 HTC in respect of U (Fixed L) 47

Figure 32 Effect of length on heat transfer performance 48
Figure 33 Oscillating dynamic observation for rectangular textile (L × W: 0.075 m × 0.102m; $f = 66.67\ Hz$ (T ≅ 0.015 s) , highlighted dot is used for tracking its dynamic traces.) 50
Figure 34 Oscillating dynamic observation for rectangular textile (L × W: 0.075 m × 0.064m; $f = 55.56\ Hz$ (T ≅ 0.018 s), highlighted dot is used for tracking the traces) 50
Figure 35 Oscillating dynamic observation for rectangular textile (L × W: 0.075 m × 0.044m; $f = 76.92\ Hz$ (T ≅ 0.018 s), Highlighted dot is used for tracking the traces) 51
Figure 36 Oscillating frequency f in respect of inlet wind velocity $U\infty$. Legend in unit: cm 52
Figure 37 Oscillating frequency f in respect of textile area coverage ratio $A*$ 56
Figure 38 Typical phenomena during irregular oscillations 57
Figure 39 Irregular oscillating dynamic observation for rectangular textile 58
Figure 40 Irregular oscillating dynamic observation for rectangular textile 59
Figure 41 K related to the flow-induced oscillation frequency. 64
Figure 42 K related to the flow-induced oscillation frequency labeled by various colors. 65
Figure 43 Flow-induced oscillation frequency in respect of textile area coverage ratio. 66

Nomenclature

a, b, h	Dimensional parameters for selected triangle and trapezoid shape flexible structures
A	Area
A^*	Area ratio of the flexible structure to total heat transfer area
$A_{textile}$	Area of selected flexible structures
$A_{heat\ transfer}$	Total area of on the hot plate affected by convective cooling
D_H	Hydraulic Diameter of the Wind Tunnel
f	Oscillating frequency
f_D	Darcy friction factor
f^*	Flow-induced oscillation frequency
h	Average heat transfer coefficients
L	Lengths of selected rectangular oscillating structures
Nu	Nusselt number
Pr	Prandtl Number
Q_{input}	Dissipated power
Re	Reynolds number

T	Oscillating time period for one oscillating cycle
$T_{surface}$	Temperature measured at steady state hot plate surface
T_{inlet}	Airflow temperature measured at the inlet of vertical wind tunnel
U_{∞}	Inlet wind velocity
W	Widths of selected rectangular oscillating structures
ρ	Air density

Chapter 1: Introduction

*1.1 **Background***

Considerable research has been conducted to study and enhance air-side convective heat transfer in various applications [1]–[10]. In the meantime, many experimental studies has been done to focus on the flow properties and thermal parameter charactrizations in different conditions [11]–[14]. Heat transfer through enhanced convective methods are useful for many industrial applications, which have been widely studied for the associated performance gains. Several concepts, including destabilizing the shear layer, disrupting the growth of boundary layers, and increasing the turbulence intensity have been widely investigated [15].

Convective heat transfer has been improved by strengthening the turbulence within the boundary layer near the wall surface with the use of rigid vortex generators [16]–[18]. RVGs have been applied to various industrial applications, as reviewed by Jacobi and Shah, different RVGs have been compared for the designs and applications, as shown in Fig.1 [18]. The heat transfer coefficient (HTC) was found to increase from $95\ (\mathrm{W}/(\mathrm{m}^2 * \mathrm{K}))$ in the plain surface to $120\ (\mathrm{W}/(\mathrm{m}^2 * \mathrm{K}))$ with louver vortex generator, and the geometry change between vortex generators could also lead to a 10% ~ 20% difference in HTC increasing. [17] Moreover, for the channel flows and flat plate, Gentry and Jacobi have studied the vortex generator enhanced heat exchange performances, which provided an experimental data of 55% enhancement in averaged heat transfer coefficients (HTC) [19].

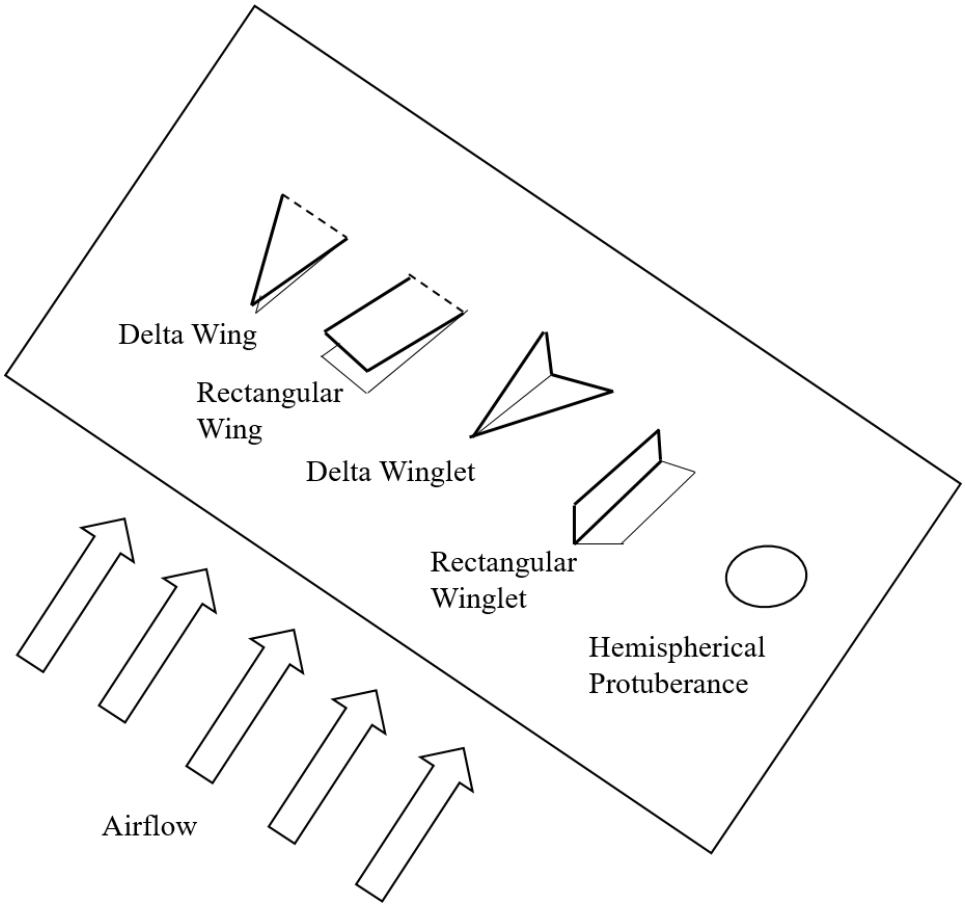

Figure 1 Common vortex generators and the associated geometrical definitions (Adapted from reference [18])

It was also reported that over 90% of the patents regarding enhancements on fin and tube heat exchangers are related to interrupted surfaces in several review papers by Wang et al. [16, 17] For the RVG designs, geometry optimization have been considered to be one of the key factors, for example, Fig.2 demonstrates a design of semi-dimple vortex generators, which have been experimentally compared to other vortex generators by Wang et al. [20]

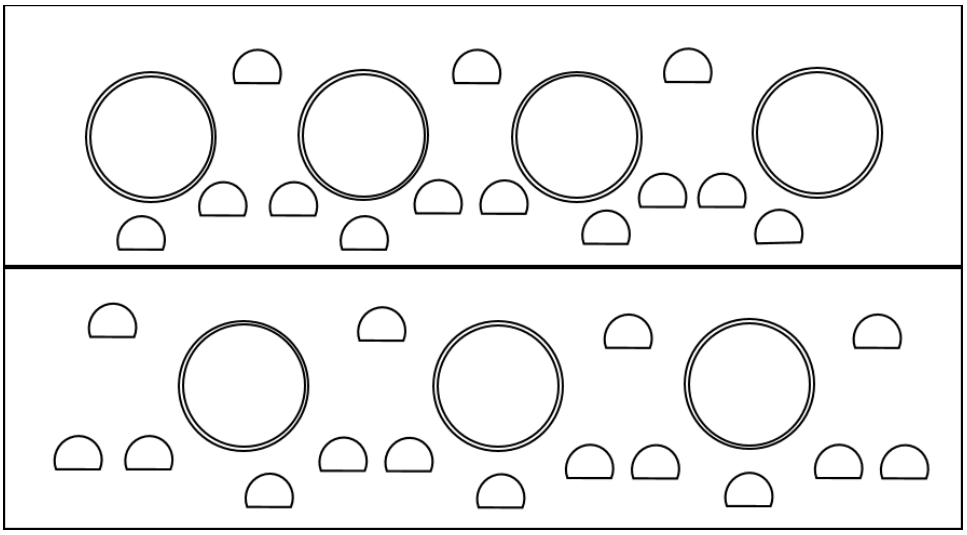

Figure 2 Schematic illustration for a semi-dimple vortex generators (Adapted from reference [20])

Compared to RVGs, recent research has proposed the idea of freely oscillating Flexible Vortex Generators (FVGs) aimed to incorporate benefits from both passive vortex generators and the structural oscillation. This concept design did not require an additional external source of energy, and it could be applied to multifunctional heat exchangers/ reactors. The idea was originally proposed by Ali et al. [21], and the design schematic is shown in Fig. 3. They reported that the quality of the mixture was enhanced up to 98% compared to the rigid case, along with 96% increase in Colburn factor, 56% in thermal performance factor, and 134% increase in the overall heat transfer [21]. A recent research by Li et al. developed an airfoil-shaped self-agitator, which numerically showed 52% improvements on Nusselt number at the same Reynolds number and experimentally presented 34% improvements on Nusselt number at the same Reynolds number [22].

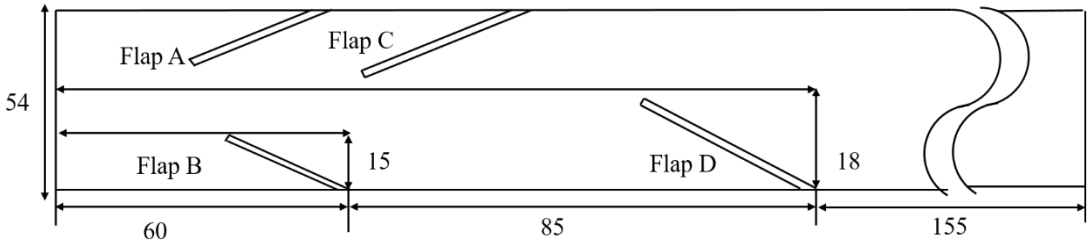

Figure 3 Schematic illustration of computational domain for FVG simulations by Ali (Dimensions in mm; Adapted from reference [21])

Similar to the FVGs mentioned above, heat transfer can be enhanced by unsteady flow with disrupting the boundary layer and this leads a better mixing with the core flow. Several other researchers have also been focusing on the HTC enhancements by generating unsteady flows, and two of the successful methods are the application of oscillating piezoelectric fans and vibrating reeds [23-30].

In previous experimental and numerical studies, Acikalin et al. investigated the cooling performance of piezoelectric fans in an enclosure of conventional cellular phones and laptops, and they found that the piezoelectric fans can offer significant localized cooling, which exceeded 100% HTC enhancements compared to natural convective cooling. [23] Another research conducted by Acikalin et al shows that the HTC enhancements exceeded 375%, and the temperature drop was more than 36.4℃, for the best case with piezoelectric fans [24]. The schematic diagram for that experimental diagram is shown in Fig. 4.

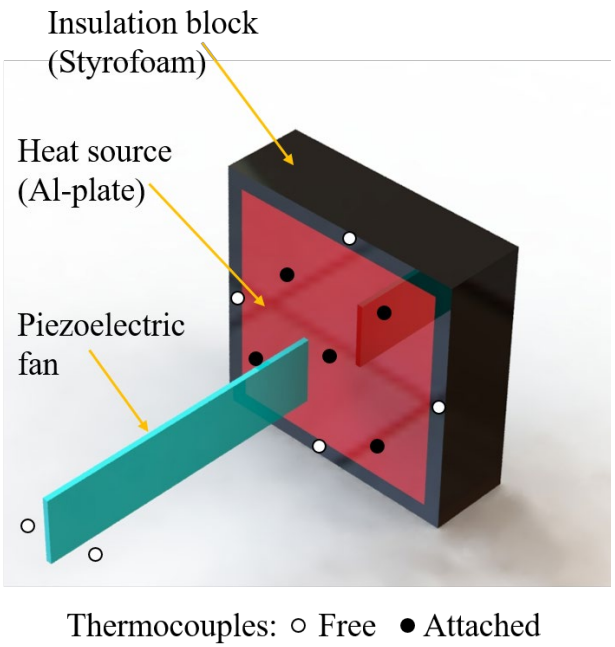

Figure 4 Schematic for piezoelectric fan experiments (Adapted from reference [24].)

Sydney et al. [25] reported that under high resonance modes operations, detailed piezoelectric fans induced flow around those fans were visualized under different frequencies. Those flow visualizations were achieved by applying smoke seeded flow and digital cameras, and 4 modes in total were included in the visualization. In a research by Yoo[26], several tests were executed to indicate the shape of the piezoelectric fan and its relationship to the tip displacement under certain resonant frequency. They also conducted the experiments regarding the dimensions and its resonant frequency.

Researchers have studied the effects of passive or active oscillating reeds for HTC enhancements. In phase I of Gerty's Ph.D. dissertation [27], the fluidic-driven cooling methods have been applied to a heated duct that in contact with the hardware that needs cooling, and the flow characteristics were investigated with Particle Image

Velocity (PIV). Pablo et al. [28] applied active reed technology to high-power heat sinks. The schematic rendering for active reed in each channel is shown in Fig. 5. It was reported the channel's coefficient of performance can be improved 1.4 times while accounting the power consumption and pressure drop.

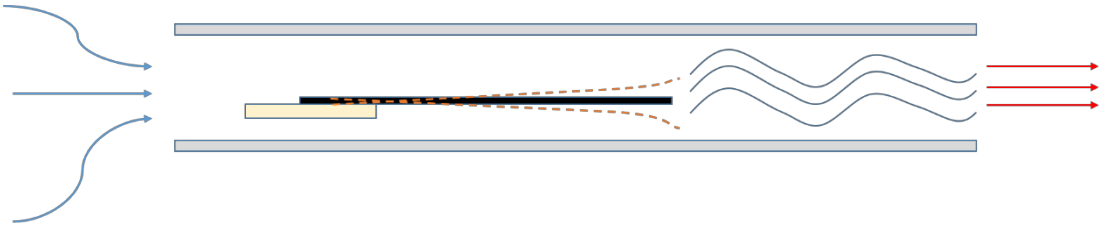

Figure 5 Schematic rendering of the flow within a channel cooled by a vibrating reed (Adapted from reference [28].)

MEMS-fabricated reeds have been utilized as flow-powered and self-oscillating actuators, which does not require any additional power and control circuits. The local enhancement factor was calculated using the ratio of Nusselt numbers(Nu) in the case with and without the reed actuator to indicate heat transfer performance. The work reported a large heat transfer improvement (250%) in microfabricated channels in a conference publication. [29] The schematic of MEMS fabricated polymer reeds is shown in Fig. 6.

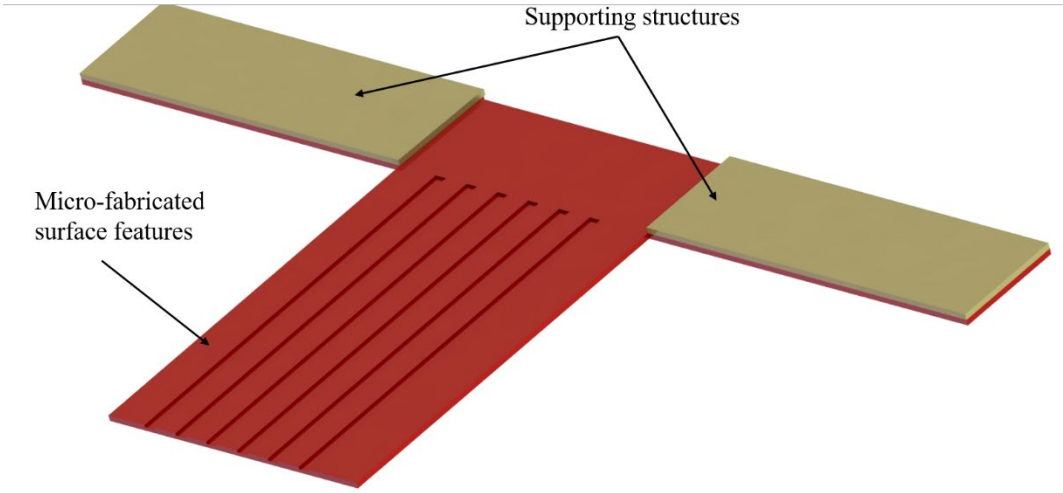

Figure 6 Schematic illustrations of laser-machined reeds with micro-fabricated surface features with micro-fabricated surface features (Adapted from reference [29])

Beside experimental studies, simulations and computational analysis have also been conducted to study flow-induced vibration of a reed in a channel, which also predicted large enhancements in thermal performances with reeds integrated [30]. Recently, thin structures with flow-induced deformability and their effect on heat transfer performance have been numerically studied and simulated [31, 32]. In 2018, Lee et al. numerically investigated the heat transfer performance in a channel flow with asymmetrically clamped flexible flags, which showed 207% increase in convective heat transfer and 135% increase in thermal efficiency factor [31]. Virot et al also systematically studied the fluttering properties of oscillating flags. [32] The unsteady flow was evaluated using the flow-induced oscillation frequency, and other dimensionless parameters were investigated for mass ratio and velocity balance. Different fluttering modes were observed for fluttering flags in their experiments. However, this study focused solely on the fluid force, and no thermal experiment was included in that experimental study.

Compared to studies on the dynamic properties of fluttering and flexible oscillating thin structures, far fewer studies have been performed to generate passive free oscillations of soft flag textiles and to discover their effect on heat transfer. The study reported in this thesis involved extensive experiments on flexible thin structures and a subsequent analysis of collected data to examine the relationship between dimensional/dimensionless parameters, the oscillating motion of flexible structures, and these structures' impact on overall heat transfer performance.

In this thesis, the experiments have been conducted using low-cost microfiber textiles as self-oscillating and flow powered structures. The plain plate heat exchanger with a flow-induced oscillating flexible textile is placed in a rectangular wind tunnel. This experiment measures the heat transfer coefficient in the heated plate for textile flaps with different shapes and sizes. The motion of textile flap is captured using a high-speed camera.

The effect of the flow-induced oscillation frequency f^*, which represents unsteadiness, on heat transfer performance is also studied. Findings indicate that rectangular flaps had the highest enhancement on convective heat transfer: the heat transfer performance improved from $113\ \mathrm{W/(m^2 * K)}$ to $161\ \mathrm{W/(m^2 * K)}$ when this shape textile flap was utilized. In addition, highest heat transfer performance was found when $0.22 < f^* < 0.32$, which can be used for future design optimizations. The experimental data are analyzed to examine the relationship between dimensional parameters, the oscillating dynamic features of flexible textiles, and these textile flaps' impact on overall heat transfer performance.

Low cost microfiber cloth are applied as flexible flow-induced self-oscillating structure. Compared to previous study, this low-cost material is commonly seen in daily life, also easy to machine and setup. The findings from this thesis research can be applied to new design of air to air plate heat exchangers, which may provide possible enhancement in the efficiency of heat transfer between airflows under different temperatures. Other possible applications area can be the pipe cooling, or new design for fin-tube heat exchanger. Further optimizations are needed for actual industrial applications.

This thesis is organized as follows. Chapter 2 introduces the experimental setup and design of the flag textiles. Chapter 3 introduces the calculating method applied in this thesis research. Chapter 4 demonstrates the experimental validations and hotplate experiments. The effects of multiple parameters and results based on various shapes of flag textiles are discussed in chapter 5 and 6. Chapter 7 concludes this experimental thesis research, and chapter 8 proposed several possible future developments.

Chapter 2: Experimental Setup

2.1 Experimental Facilities:

The experiments were conducted on the Cross Flow Heat Exchanger H351D from P.A. Hilton LTD. This equipment provide a console, several integrated sensors, a vertical wind tunnel for airflow, and an integrated flat plate that could be evenly heated, which means it obtained the ability of temperature measuring, pressure measuring, and the input power control. The overall schematic is shown in the following Fig. 7, with all specific parts labeled. As shown in the Fig. 11, the experimental setup could divided into two categories. The thermal experimental setup is shown in the Fig. 11(a), while the motion observing experimental setup, which applied the same cross flow heat exchanger is shown in the Fig. 11(b).

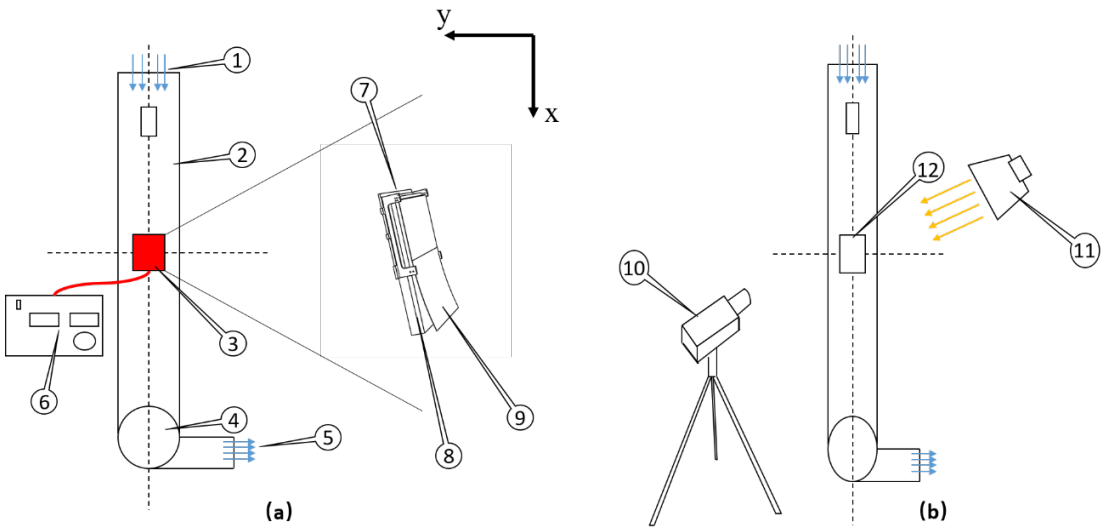

Figure 7 Schematic of experimental setup for (a) heat transfer measurement and (b) dynamics observation of textile flap

Legend: 1. air inlet; 2. vertical wind tunnel; 3. heat transfer area; 4. fan; 5. air outlet; 6. console and power supply; 7. 3D-printed supporting structure; 8. hot plate with thermal insulation foam; 9. flexible self-oscillating textile flap; 10. phantom v9 high-

speed camera; 11. white woven lamp; 12. observation window. x = wind inlet direction.

The dimension of this testing equipment was measured by a ruler and a calibrator. For the dimension of the wind tunnel, it has the length approximately of 1 [m], and a depth approximately of 0.05 [m]. The flat plate was placed at distance around 0.45 [m] from the top of this tunnel, and the total thickness of the plate is around 0.015 [m], including the aluminum hotplate thickness of 0.005 [m].The width of the hotplate is 0.127 [m] and the length of the heated plate is 0.151 [m]. The opening of the wind tunnel, which is the place for hotplate integration, has the dimension of 0.15 [m] in width and around 0.20 [m] in length. This design left only 0.025 [m] for the additional structures in horizontal direction, and even smaller space was left for additional modifications in vertical direction. Table 1 is a brief summary for the experimental facilities and equipment applied to this experimental study.

The white microfiber cleaning cloth from SecurOMax is selected to act as the flow-induced self-oscillating structures in this experimental study. The cloth is designed for lens cleaning, and the composite of this kind of fabric are 80% of polyster and 20% of polyamide, which made it have extra softness. The ignition point of polyster and polyamide generally exceeds 200 degrees, and this temperature tolerance is appropriate for this experimental study and implies a wide range of industrial application.

Table 1 Experimental facilities with its accessories

Components	Specifications	Dimensions	Materials
Vertical Wind Tunnel	Part No. P.A. Hilton LTD. Cross Flow Heat Exchanger H351	1 [m](Length) × 0.2 [m] (Width) × 0.05 [m] (Depth)	N/A
Hot Plate	This is an integrated part in model H351	0.151 [m](Length) × 0.127 [m](Width) × 0.005[m] (Height	Aluminum
Microfiber Textiles	Part No. SecurOMax SMWHT12X12MFC6PK	Cut into specific desired shapes and dimensions	80% Polyester/ 20% Polyamide
Thermocouples	OMEGA Type K	N/A	N/A
Thermometers	OMEGA HH74K	N/A	N/A
High Speed Camera	Vision Research Phantom V9	N/A	N/A
Motor/ Bottom Wind Pump	Manufacturer: Air Control Industries Limited;	N/A	N/A
White Woven Lamp	Function: Light Filling	N/A	N/A
3D Printed Structures	Function: Holding the Flexible Textiles	Thickness: 0.002 [m]	PLA/ Thermoplastic

2.2 Experimental Setup:

2.2.1 Thermal Experimental Setup

As shown in the Fig. 7(a) above, based on the experimental facilities in the thermal-fluid lab, many modifications and preparations are needed for this thermal performance enhancement experimental study. However, as mentioned above, the space left for modifications is limited, and special designs needed to fit into the space for the hotplate and this vertical wind tunnel.

To achieve this goal, the idea of 3D printed structures was raised, and a 3D printer was built using Folger Tech 2020 i3 assembly kit. The 3D printer is indicated as shown in the following Fig. 8. After configuration, this small 3D printer is ready to be use for the supporting structure manufacturing, and it provided lots of convenience throughout this experimental study.

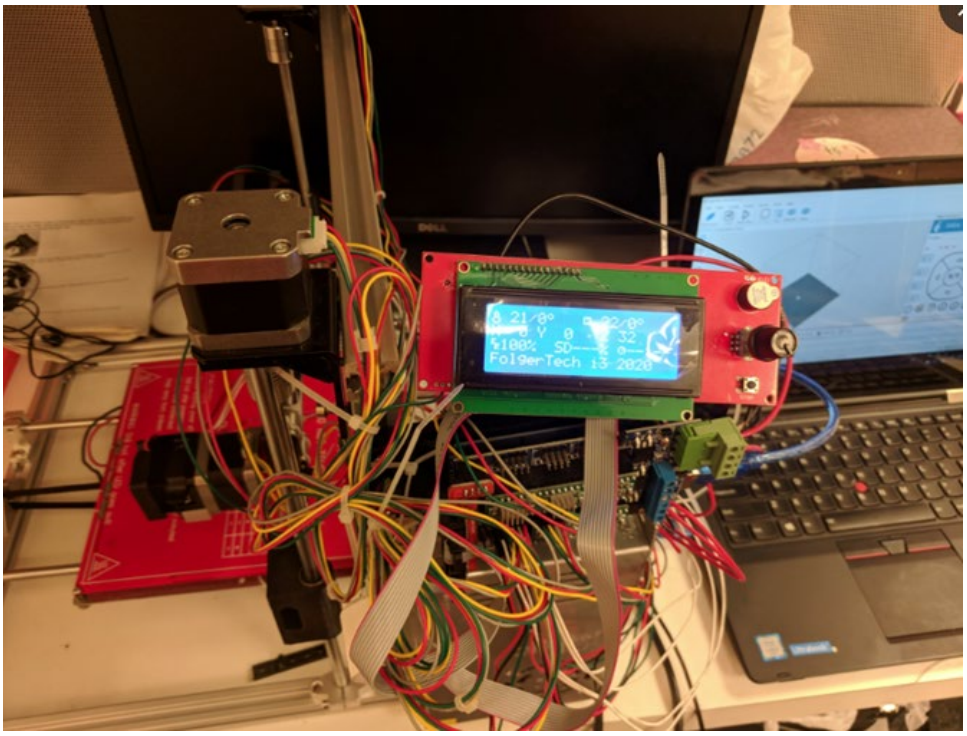

Figure 8 Desktop 3D printer Folger Tech 2020 i3

Several solid structures were designed for placing the flexible structures. The dimension left on this highly integrated industrial crossflow heat exchanger is limited. For example, the space left on 2 sides of the hot plate for adding additional structures is less than 0.012 [m], and the space left in front of the hotplate is less than 0.01 [m]. The schematics of 2 kinds of solid structures designed for holding different shapes and dimensions of flexible structures are shown in the following Fig. 9. For most of the cases, the solid structure was integrated with the hotplate, as shown in the following Fig. 10. A more detailed dimensional demonstration could also be found in the following Fig. 10. As indicated in the Fig. 10, the thickness for the side-supports are 2.25 [mm], the bottom thickness of this structure is 2.5 [mm], and the distance between the stainless steel wire and the hotplate surface is 3.78 [mm].

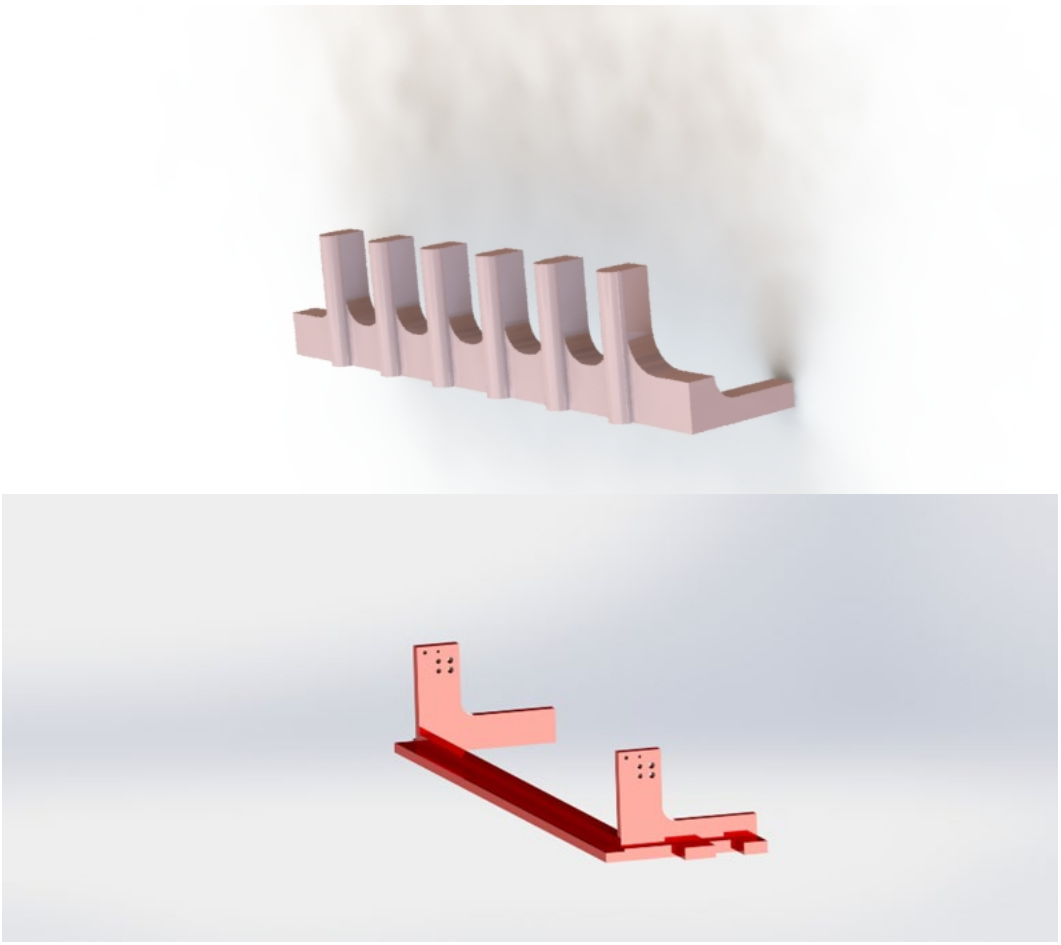

Figure 9 CAD models designed for the different flexible structure placements

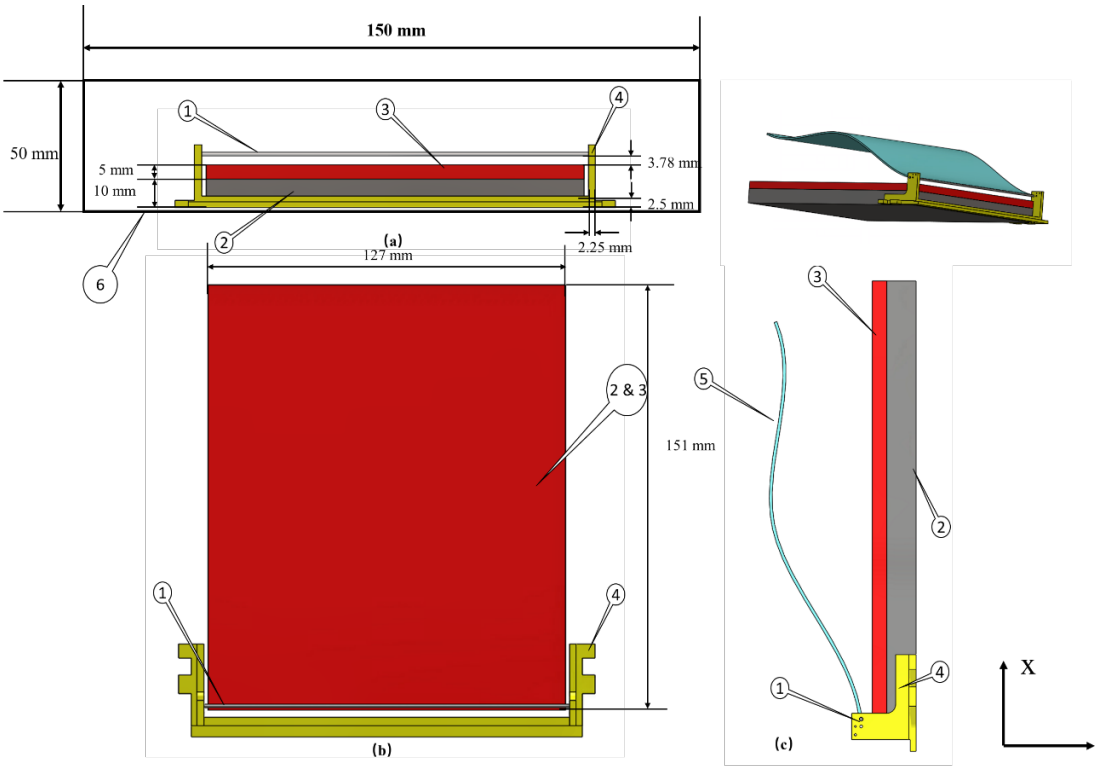

Figure 10 Integrated heat transfer area schematic.

Legend: (a). front view; (b). top view; (c). side view; 1).stainless steel wire; 2). hot plate base; 3). hot plate; 4). 3D printed structure; 5). flexible textiles; 6). wind tunnel cross section; x = wind inlet direction

As shown in the Fig. 10, this design applied thin structure along with stainless steel wire to hold the flexible structures, which did not block the airflow path. However, there is a potential structure strength issue, and it was worried that the thermal plastic structure may not hold under high wind velocity. Several tests with different wind inlet velocities U_∞ were conducted, and the final design used a straight 304 stainless steel wire and BJB epoxy to hold the hanging structure. The wind inlet velocity U_∞ is selected to be 9.9 m/s, 12.12 m/s, 14 m/s, 15.65 m/s, 17.15 m/s, and 18.52 m/s. Furthermore, for the thermal experiments, the overall experimental conditions selected in this experimental study is shown in the following Table 2.

Table 2 Selected experimental conditions

Experimental setup parameters	Input values	Additional notes
Voltage	60 [V]	
Power input	70.45 [W]	Calculated from voltage input
Wind inlet velocity	9.90/ 12.1/ 14.0/ 15.7/ 17.1/ 18.5 [m/s]	Calculated from manometer readings, using bernoulli equation
Wind inlet temperature	~22 [℃]	Normally the same as room temperature, also measured at the wind tunnel inlet.

As shown in the Fig. 11 is the schematic for dynamic properties observation experimental setup through the high speed camera. In this setup, the hot plate was taken out from the original integration, and acrylic sheets (PMMA) with same dimensions were placed there to visualize the oscillation of the textiles.

Several tests have been conducted to test the effects of the 3D-printed solid structure. Including the pressure drop comparison and wind inlet velocity test. The pressure measurement testing setup is shown in the following Fig. 11. In the meantime, Fig. 12 shows the pressure drop comparison between the case that 3D printed structures were added and the pressure drop with only hotplate integrated. It seems the 3D printed supporting structure did not have much effects on the overall pressure drop.

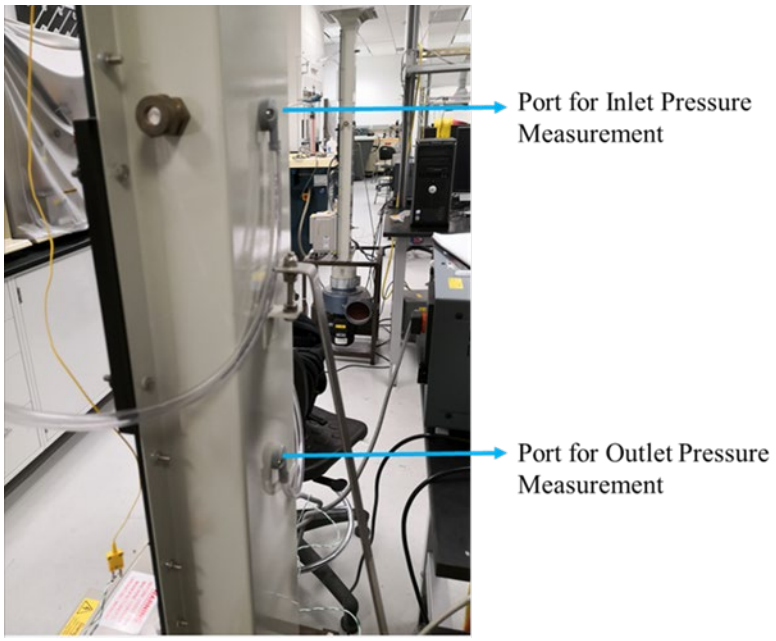

Figure 11 Pressure drop measurement setup

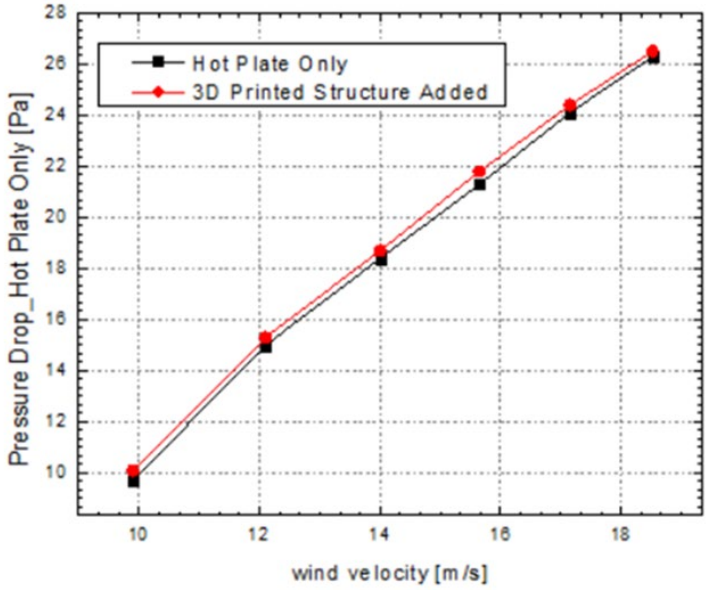

Figure 12 Pressure drop comparison between 1). Hotplate only; 2). 3D printed solid structure added

2.2.2 Dynamic Observation Experimental Setup

The Fig. 7(b) is the schematic for dynamic motion observation experimental setup through the high speed camera. In this setup, the hot plate was taken out from the

original integration, and acrylic sheets (PMMA) with same dimensions were placed there to visualize the oscillation of the textiles. Compared to the thermal experiments, the dynamic observations were conducted in the same wind tunnel with the same 3D-printed solid structures and active flexible structures. The Fig. 13 indicates a direct view after replacing the hotplate with transparent PMMA as an observation window, and one flexible textile was added to that part.

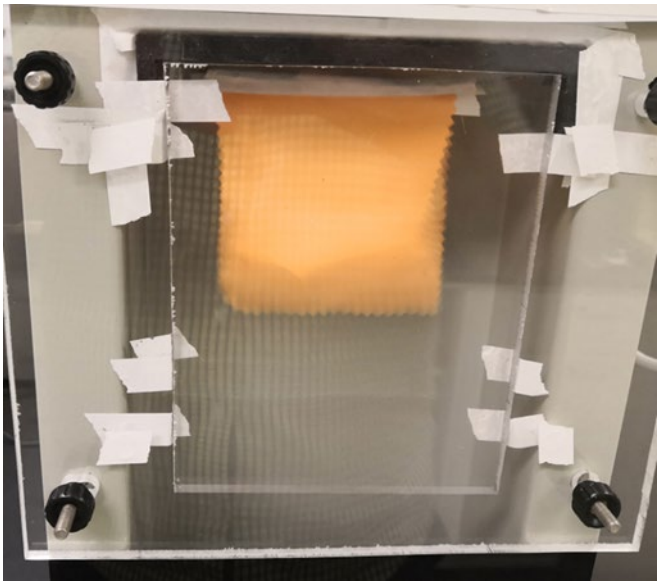

Figure 13 Visualization of experimental platform

As shown in the Fig.7. (b), part 10, oscillating frequency is observed through high speed camera Vision Research Phantom v9. A white woven lamp was applied here for the light fill purpose also shown in the schematic above shown as part 11 in the figure. The high speed camera has the ability to capture 1000 frames per second at its highest resolution of 1632×1200 active pixels. The highest frames per second could reach 153846 with the lowest resolution. In our case, around 1600 figures were

captured under the settings of sample rate being 1000 frames per second and the resolution of 1632×1200 active pixels.

The PCC Software downloaded from the Vision Research official website was applied for high speed video recordings, which could provide frame by frame observations at a time step of 0.001 seconds after the high speed camera video was recorded. Fig. 14 is the screenshot of the PCC software user interface during the observation of the textile flap motion.

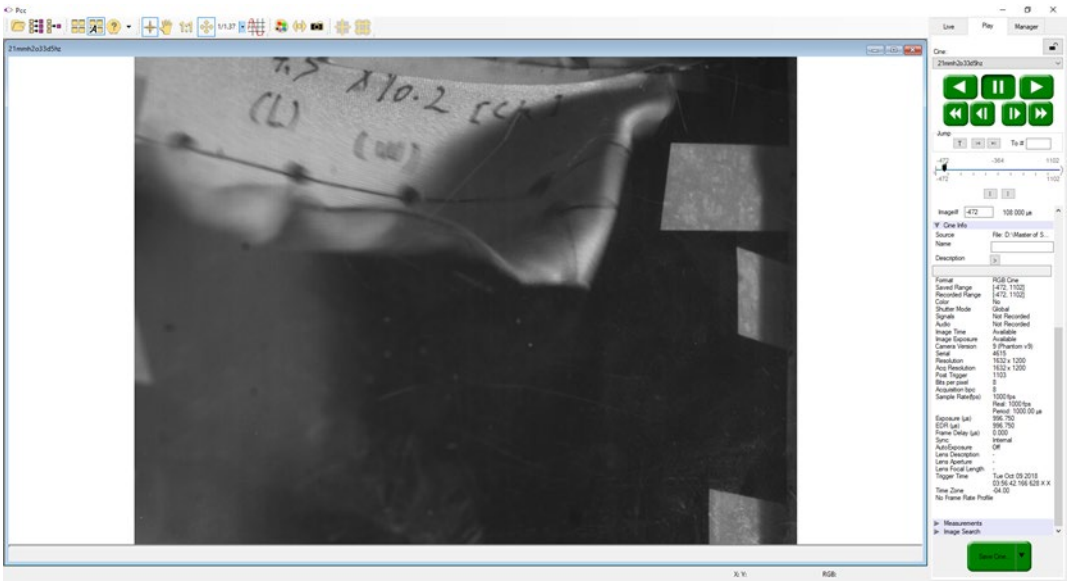

Figure 14 Vision research PCC software interface

Chapter 3: Calculation Methods

3.1 Calculation Methods

The heat transfer performance comparison in this experimental study is based on the heat transfer coefficient (HTC) calculation, which is given by the following equation:

$$\dot{Q_{input}} = h \times A \times \Delta T \qquad (1)$$

Therefore,

$$h = \frac{\dot{Q_{input}}}{A \times \Delta T} \qquad (2)$$

where the Q_{input} is the voltage input from the control panel, calculated using the known resistance, $51.1\ Ohms$, and the voltage input was selected to be $60\ Volts$ after several times of approaching, and the $\dot{Q_{input}}$ could be calculated to be 70.45 Watts.

ΔT is the temperature difference between the hotplate and surrounding fluid temperature. Both temperatures were measured through K-type thermocouples, and the thermometer applied here is the Omega thermometer HH74K. In this case, due to the experimental limitations, the surrounding fluid temperature is replaced by the term of wind inlet temperature.

$$\Delta T = T_{surface} - T_{inlet} \qquad (3)$$

At the beginning, the experiments were run based on the flat plate only situation. The wind speed was calculated using the Bernoulli equation, which applied the pressure reading from the manometer at the top of this tunnel. The equation is shown as the following:

$$p_{total} = p_{static} + \frac{1}{2}\rho_{air} U_{\infty}^2 \qquad (4)$$

In which, the $p_{total} - p_{static}$ could be represented by the height of water indicated on the manometer, with the unit of millimeter-water. Therefore, the equation could be simplified as follows:

$$\frac{1}{2}\rho U_{\infty}^{2} = \rho_{water} g \Delta h_{water} \quad (5)$$

Through trial and error, the Δh_{water} in the equation above was selected as follows: 6 mmH_2O, 9 mmH_2O, 12 mmH_2O, 15 mmH_2O, 18 mmH_2O, and 21 mmH_2O, and correspondingly, the inlet wind velocity is 9.9 m/s, 12.12 m/s, 14 m/s, 15.65 m/s, 17.15 m/s, and 18.52 m/s.

Although only one side of the wall has the protruding and heated hotplate, the actual airflow condition should be considered as channel flow condition. The constant volume flow was compressed when passing the heat transfer area, because of its protruding feature. Except the airflow passing through the sides of the hot plate, the hotplate was mainly compressed by the height occupation. The height of the hotplate and its base occupied around 3/10 of the entire channel depth, and reversely, the wind velocity increased by 10/7. As shown in the following, and the increased wind velocity at hotplate entrance became 14.14 m/s 17.32 m/s 20m/s , 22.36 m/s24.49 m/s and 26.46 m/s Therefore, for correlation, the Reynolds number under this case is calculated using the equation below:

$$Re_L = U_{\infty} \times \rho \times \frac{D_H}{\mu_f} \quad (6)$$

Where $U_{entrance}$ is the wind velocity after the compression of the air flow, D_H is the hydraulic diameter, and it could be calculated using the equation $D_H = \frac{2ab}{a+b}$, and a, b is the dimension of that compressed channel.

The friction factor across the test section (or arbitrary distance L_c) is estimated as:

$$f_D = \frac{2D_H}{L_c} \times \left(\frac{\Delta P}{\rho * U^2}\right) \qquad (7)$$

Nusselt numbers were also calculated for correlation purposes. The experimental Nusselt number is calculated using the equation below, where h is the heat transfer coefficient, D_H is the hydraulic diameter, and k_f is the thermal conductivity of the fluid material, which is air in our case.

$$\mathrm{Nu} = (\mathrm{h} \times D_H)/k_f \qquad (8)$$

For the turbulent channel flow convective heat transfer, the method of Gnielinski correlation [33] was applied in this experimental study, as shown below:

$$Nu_{correlation} = \frac{\left(\frac{f_D}{8}\right)\times(Re_D - 1000)\times Pr}{1+12.7\times\sqrt{\frac{f_D}{8}}\times\left((Pr)^{\frac{2}{3}}-1\right)}\left[1+\left(\frac{d}{l}\right)^{\frac{2}{3}}\right] \qquad (9)$$

In which, Re_L is the Reynolds number got above, D_H is the equivalent diameter, and Pr is the Prandtl number, which was assumed to be 0.71 in our case.

In this experimental study, the comparison evaluated the relationship between HTC performance and flow-induced oscillation frequency, and coverage ratio. The flow-induced oscillation frequency f^* is given by the following equation:

$$f^* = \frac{L*f}{U_\infty} \qquad (10)$$

In this equation, the L is length of rectangular textiles, f is the circular frequency, and U_∞ is the flow velocity.

Moreover, the coverage area of textile to the total heat transfer area is also important, and the flexible structure length to the wind tunnel depth. Those ratios were represented as shown in the following equations for dimensionless analysis:

$$A^* = \frac{A_{textile}}{A_{heat\ transfer}} \qquad (11)$$

3.2 Repeatability and Uncertainty Analysis:

The repeatability of the measurements is also affected to some extent by the textiles placement and materials with in the channel. However, those parameters were not included in the present thesis research. The present experimental facilities are highly integrated, and there is a large difficulties to make modification on it to achieve entire transparent constructions. Besides, those modifications or examinations for various materials testing or the effects of flexible structure placement would be time costing and expensive. Based many limitations at the current stage, those parameters were considered as parts of the future work recommendations.

Secondly, the experimental measurements uncertainty could be represented by standard deviations for the experimental error gathered from each part, which is consist of 2 parts, systematic uncertainty and random uncertainty.

$$\varepsilon_{total} = \varepsilon_{sys} + \varepsilon_{STD} \qquad (12)$$

Where:
$\varepsilon_{total} = total\ uncertainty\ of\ a\ measured\ valure$
$\varepsilon_{sys} = systematic\ uncertainty\ of\ a\ measured\ valure$
$\varepsilon_{STD} = random\ uncertainty\ of\ a\ measured\ valure$

$$\varepsilon_{STD} = \sqrt{\left(\left(\sum_{j=1}^{N}\left(x_j - \bar{x}\right)^2\right)/(N-1)\right)} \qquad (13)$$

Where:
$N = number\ of\ data\ points\ in\ the\ collected\ data\ set$
$j = data\ point\ index$
$x_j = measured\ variable\ data\ point\ at\ index\ j$
$\bar{x} = average\ of\ the\ measured\ variable\ over\ the\ entire\ data\ set$

In this case, we are focusing on the HTC measurements and evaluations, which is consisted of 3 parts. The uncertainty of dimension measurement, the uncertainty of temperature measurements, and the uncertainty of power input.

The system uncertainty in the measured dimension, the length and width, is 1 mm or 0.8%, respectively. The uncertainty in $T_{surface}\ and\ T_{in}$ is supposed to be 2.2 ℃ or 0.75%, The power output is calculated as the product of voltage output from the console, the uncertainty is estimated to be 1%. Therefore, the highest uncertainty for the air-side averaged HTC should be $\pm 7\%$. Based on the hotplate experiments, this experimental study obtain the largest random uncertainty $\varepsilon_{STD} \sim \pm 4\%$, and the maximum $\varepsilon_{total} \sim \pm 11\%$.

The facility obtain a thermal insulation layer under the aluminum hotplate, and the power input calculated using the heat capacity formula ($\dot{Q} = \dot{m}c_p\Delta T$) of air flow had a good agreement with the console power input. Therefore, the teat loss in this thesis research were considered to have minor influences on experimental results and not included in the calculation and uncertainty analysis.

Chapter 4: Hotplate Experiments for System Validation

This experimental study started with the cases that used forced convective cooling over the hotplate without any additional structures. Under the selected experimental conditions, Table 3 shows the experimental data for flat plate convective heat transfer experiments. The experimental sets were duplicated 3 times, and they were in good agreement with each other. Table 4 indicates the corresponding heat transfer coefficients calculated from those cases. The average heat transfer coefficient calculated from experimental data was in the range of 70.15 $\mathrm{W/(m^2.K)}$ to 120.40$\mathrm{W/(m^2.K)}$. Fig. 15 is the plots for the heat transfer coefficient experimental data of hotplate experiments, the error bar there was indicating the random uncertainty, ε_{STD}.

Table 3 ΔT gathered from flat plate experiments

Upstream Wind Speed [m/s]	Reynolds Number (Re)	ΔT_1 $[°C]$	ΔT_2 $[°C]$	ΔT_3 $[°C$	$\Delta T_{average}$ $[°C]$	ε_{STD} $[°C]$
9.9	5.47×10^4	44.3	44.9	47.9	45.7	1.90
12.1	6.70×10^4	37.9	37.8	38.2	38.0	0.21
14	7.73×10^4	32.9	33.4	31.9	32.7	0.76
15.7	8.64×10^4	30.3	29.8	30.5	30.2	0.36
17.1	9.47×10^4	28.8	27.9	27.5	28.1	0.67
18.5	1.02×10^5	27	26.5	26.3	26.6	0.36

Table 4 HTC of flat plate experiments

Wind Speed [m/s]	Reynolds Number (Re)	h_1 $[\mathrm{W/(m^2.K)}]$	h_2 $[\mathrm{W/(m^2.K)}]$	h_3 $[\mathrm{W/(m^2.K)}]$	$h_{average}$ $[\mathrm{W/(m^2.K)}]$	ε_{STD} $[\mathrm{W/(m^2.K)}]$
9.9	5.47×10^4	66.9	72.3	71.3	70.2	2.87
12.1	6.70×10^4	83.8	84.5	84.7	84.3	0.47

14	7.73×10^4	100.4	97.3	95.9	97.9	2.30
15.7	8.64×10^4	105.0	105.7	107.5	106.0	1.29
17.1	9.47×10^4	116.4	111.2	114.8	114.1	2.66
18.5	1.02×10^5	121.8	118.6	120.8	120.4	1.64

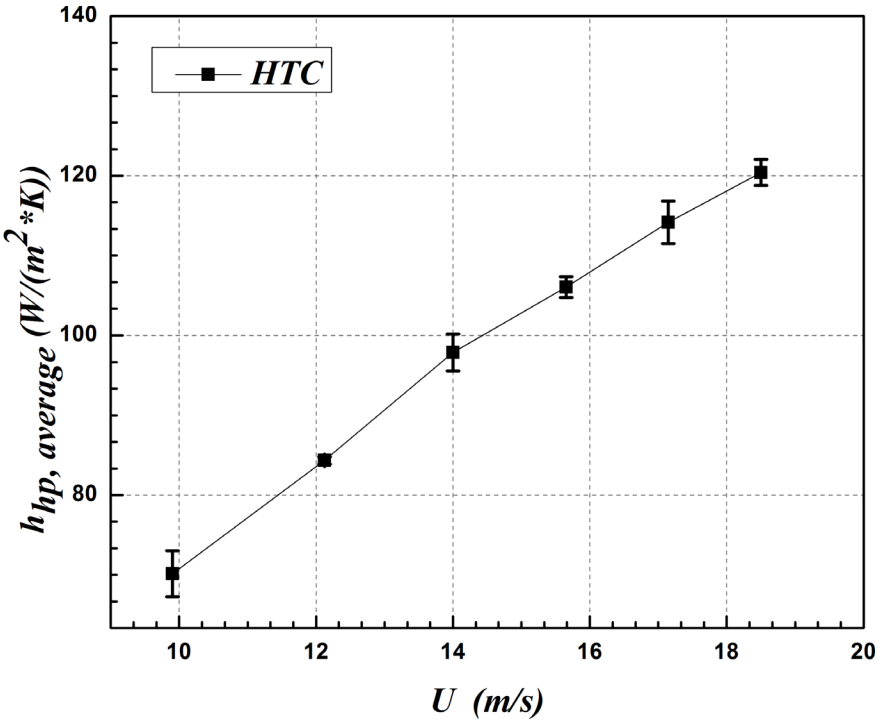

Figure 15 HTC performance for hotplate experiments

With the correlating equations and methods introduced in the chapter of calculation and correlation, Fig. 16 and Table 5 shows the comparison between the Nusselt number calculated from experimental data and the Nusselt number calculated from the Gnielinski correlation. From those comparisons, the value found from $\frac{\mathrm{Nu}_{\mathrm{experimental}}}{Nu_{correlation}}$ is in the range of 0.896 to 0.923, and the ratio had a standard deviation of 0.012.

Therefore, under the channel heat transfer assumption, values found from the correlation equation are within an acceptable deviation compared to the experimental

data, and it shows that the channel flow convective heat transfer correlation can be applied to this experimental study.

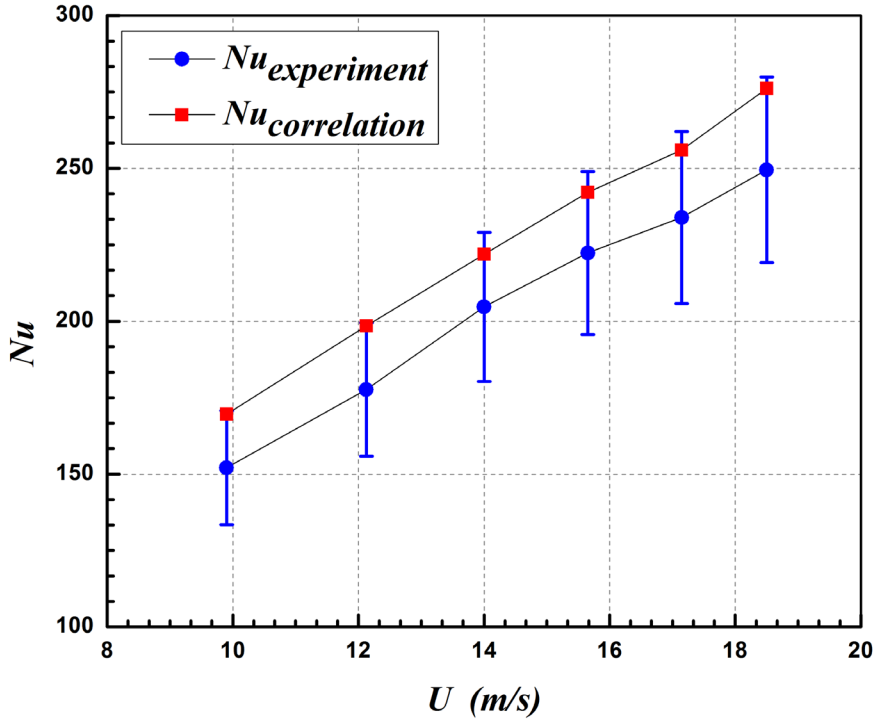

Figure 16 Comparison between $Nu_{experimental}$ and $Nu_{Gnielinski\ Correlation}$

Table 5 Comparison of the Nu from Ginelinski correlations and experimental data

Wind Velocity at Hotplate Entrance [m/s]	Re_{DH}	$Nu_{Experimental,Averrage}$	$Nu_{Ginelinski\ correlation}$	$\frac{Nu_{exp}}{Nu_{correlation}}$
14.1	145330.1	152.1	169.6	0.89
17.3	149702.1	177.7	198.5	0.89
20.0	172861.1	204.7	221.9	0.92
22.4	193264.6	222.3	242.1	0.92
24.5	211710.8	233.9	256.0	0.90
26.5	228673.8	249.5	276.1	0.90

After comparing the hotplate experimental results to the correlating equation calculated results, the Computational Fluid Dynamics (CFD) software ANSYS Fluent model was applied to simulate the experimental conditions and HTC performance. The simulation was run using the actual experimental setup geometry, which used the aluminum as the hotplate material, and the fixed wind inlet velocity recorded from the top manometer used as velocity inlet boundary condition. The flow of the complete simulation setup including the steps followed: I. Geometry Building, II. Meshing; III. Model Selection and Solution Setup; IV. Post Processing. [34]

The simulation results for 6 inlet wind velocities settings are indicated in Table 6, and in the Fig. 17, the flow was represented using streamlines, and the surface temperature on the flat plate was monitored after the convection heat transfer reached the steady state. The inflation was applied to describe the boundary layer, and the first layer thickness was approximately set. The maximum boundary layer thickness in this case can also be estimated using the formula for turbulent flow over a flat plate, which

obtained around $0.004\ m$ at the end of hotplate. This value is applied to the inflation settings in ANSYS mesh setup.

The viscous model applied in this case was based on the calculated Reynolds number is Transient SST model, and the wind inlet temperatures used experimentally measured inlet temperatures, which were recorded using a K-Type thermocouple placed in the wind tunnel inlet. The following figures indicated the velocity simulation results for the experimental setup of the hotplate only cases. Table 6 is the comparison between the ΔT computed from the ANSYS simulation and $\Delta T_{average}$ calculated from the experimental results. Those simulating results showed an acceptable agreement with the data got from experimental results.

Table 6 Temperature differences monitored from simulating results compared to average experimental data

Upstream Wind Inlet Velocity [m/s]	$\Delta T\ from$ Simulation [°C]	$\Delta T\ from$ Experimental Results [°C]	$\frac{\Delta T_{simulation}}{\Delta T_{experimental}}$
14.1	43.9	45.7	0.96
17.3	38.9	37.9	1.02
20.0	34.7	32.7	1.06
22.4	31.6	30.2	1.05
24.5	29.3	28.1	1.04
26.5	28.9	26.6	1.08

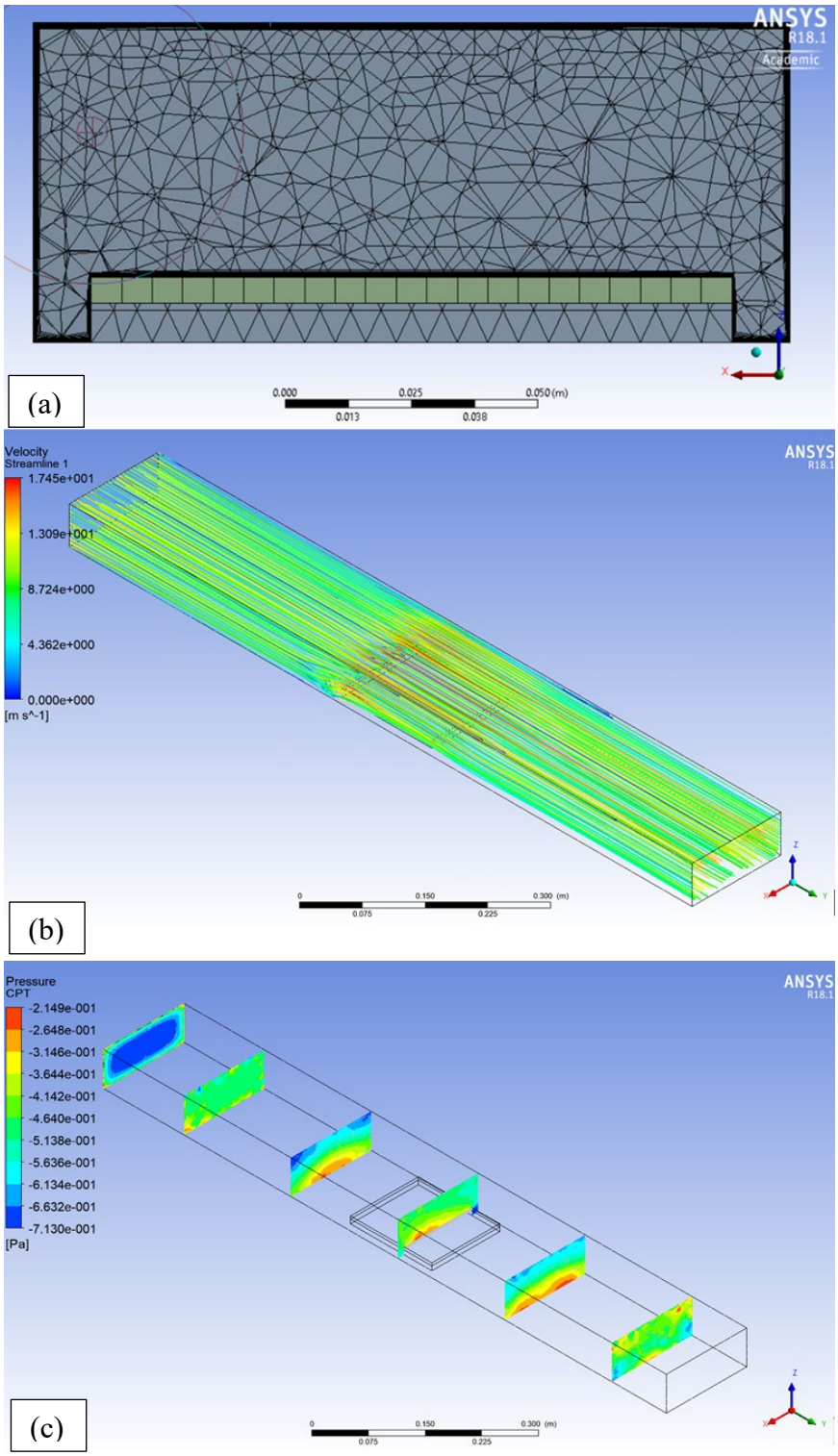

Figure 17 ANSYS fluent simulation interface and sample results (from top to bottom): a). Mesh setup (with inflation to indicate boundary layers); b). Sample Simulation Results (Velocity streamline under the situation of velocity inlet of 9.9 m/s); c). Cross surface local pressure rendering

There are also uncertainties in the simulation, and the difference between the ANSYS simulation and the experimental data may come from the following sources, as reported by other researchers in the following Table 7 [34].

Table 7 Source of uncertainty and error in CFD simulations

(Summarized from the references [34])

Source	**Examples**
physical modeling	chemical reacting flow transitional flow inviscid flow
auxiliary physical models	equation of state thermodynamics properties transport properties chemical models
initial and boundary conditions	wall roughness far-field free-stream condition
discretization and solution	truncation error iterative convergence – steady state and time dependent
round- off error	finite – precision arithmetic
programing and user part	

After the validation through hotplate experiments, the appropriate correlation can be selected. This correlation can be utilized in the textile design after specific simplifications and adjusts. Following steps were focusing on the effects of adding flexible structures above the hotplate.

Chapter 5: Effects of Different Shapes

5.1 Effects of Small Stripes

At the beginning of this experimental study for the effects of flexible structures, textiles were cropped into small sheet structures were tested. The materials were cut into 12 pieces with 2 mm in width (in horizontal placement) and 10 mm in length. The goal of this was to investigate small and separate oscillation effects on the fluid domain and their effects on the heat transfer domain. The first setup of the experiment used separated small oscillation pieces as shown in Fig. 18. The experimental data compared to the flat plate experiments are plotted in the Fig. 19.

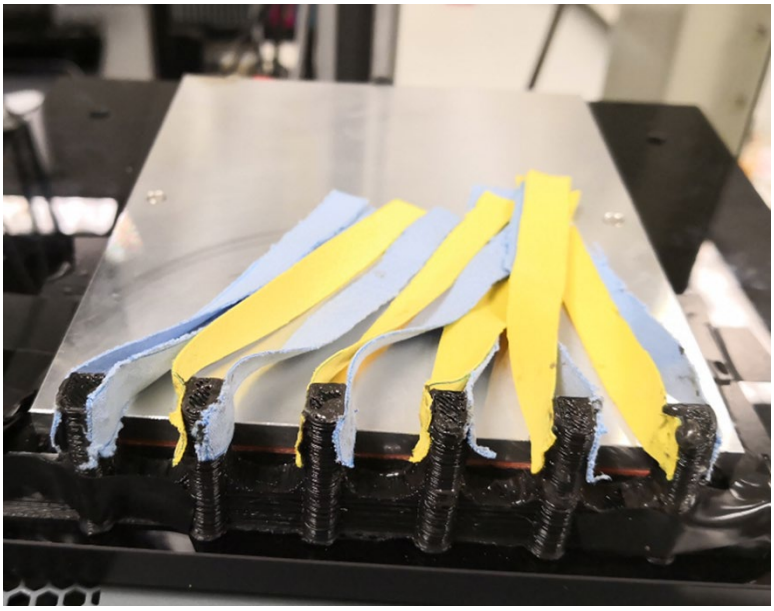

Figure 18 Initial Trying of Using Small Self-Oscillating Rectangular Sheets

It turns out that a better heat transfer performance could be achieved by adding the strips to the flat plate under the same upstream inlet wind velocity, which provided the confidence for the following experimental studies. The explanation of this

phenomenon could be the increased turbulence in the fluid domain inside the channel and a better mixture of the airflow. However, in this case, the pillow structures at the front of the solid design also played an important role in respect of the heat transfer performance. However, the oscillating motion of this kind of strips is difficult to observe through high-speed camera, and those pillow structures generated many limitations for further experiments.

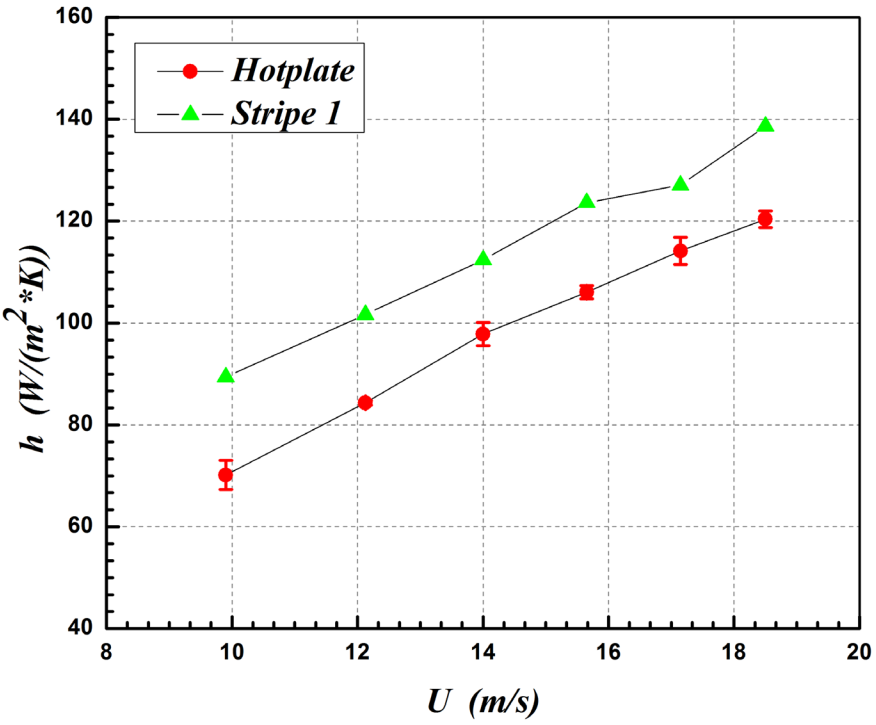

Figure 19 Experimental results of the initial approach on stripe structures

Another kind of strip structure, as shown in the Fig. 20 was also tested. This kind of design and orientation applied the designed solid structure described the experimental setup section. The strip were cut into 7 pieces with 0.01 [m] in width, and 0.14 [m] in length. Heat transfer coefficients were calculated for thermal performance

comparison. However, the experimental results showed that the small sheets of flexible structures did not effectively change HTC values.

1. Stainless Steel Wire;
2. Hot Plate Base;
3. Hot Plate;
4. 3D Printed Structure
5. Stripe Structures ($7 \times 0.01 \times 0.14$ $[m]$)

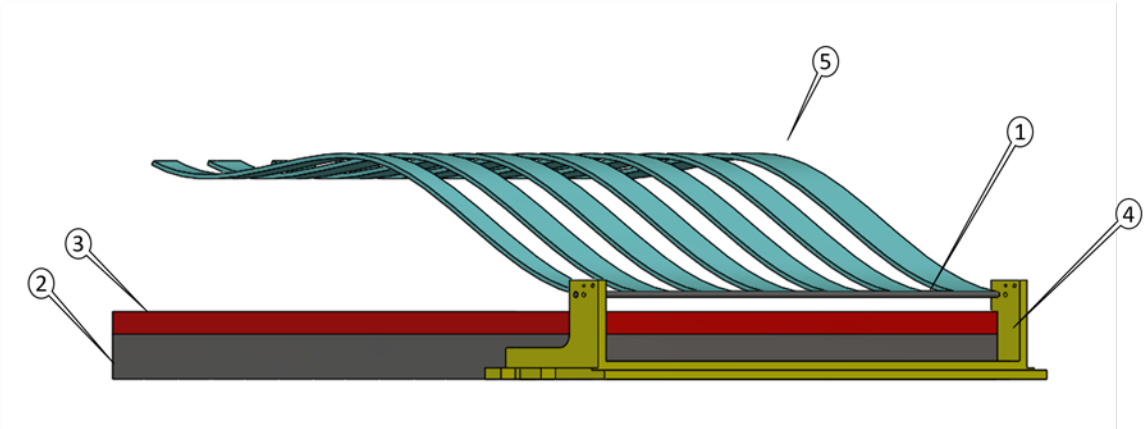

Figure 20 Stripes on hotplate schematic

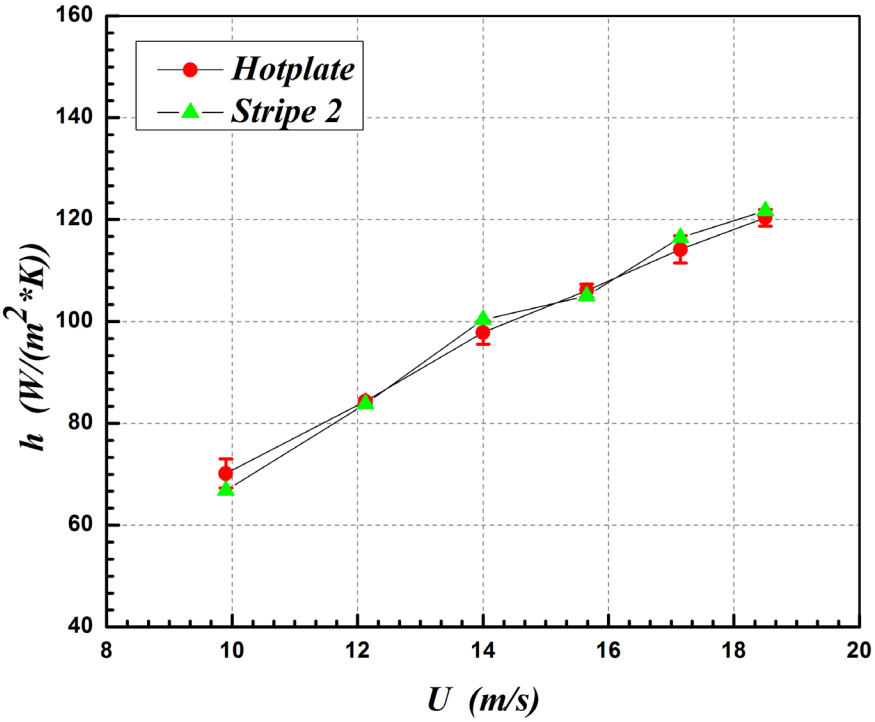

Figure 21 Experimental results of the second approach on stripe structures

5.2 Effects of Various Shapes

5.2.1 Design of Various Textile Shapes

In the following experiments, various shapes were tested under the same wind inlet conditions. From the experimental results, it was found that the rectangular flexible sheets(shape (1)) that covers a relatively large percentage of the heat transfer area, could offer a heat transfer coefficient enhancement of 36% compared to the hot plate only case. The following Fig. 22 indicated all the different shapes and dimensions tried at the beginning of this experimental study.

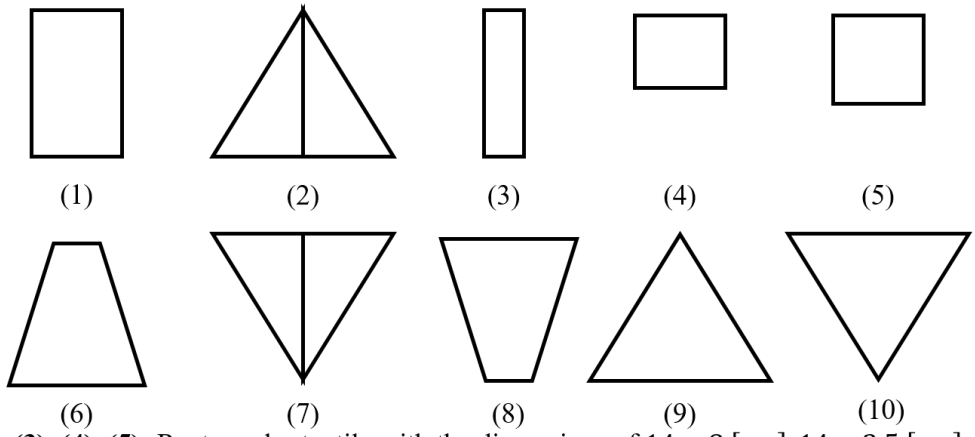

(1), (3), (4), (5): Rectangular textile with the dimensions of $14 \times 8\ [cm]$, $14 \times 3.5\ [cm]$, $7 \times 8\ [cm]$, $and\ 8.5 \times 8\ [cm]$;

(9), (10), (2), (7): Triangle textile with the overall dimensions of $14\ [cm](height) \times 16[cm](width)$ in different orientations;

(6), (8): Trapezoid with the dimension: $4[cm](top) \times 12[cm](bottom) \times 14[cm](height)$ under opposite orientations;

Figure 22 Schematic of different structure shapes

As shown in the Fig. 22, the selected shapes of textile included: rectangular, isosceles trapezoid, invert isosceles trapezoid, isosceles triangle, and invert isosceles

triangle. Some of them are different shapes with the same textile coverage areas, while others are the initial test of rectangular shape textiles with different length and width.

5.2.2 Effects of Various Shapes Textiles

As shown in the Fig.22 above, structure (1), (3), (4) and (5) are rectangular in shape but with different coverage areas, while the rest of structures tested are under the same coverage area ($14[cm] \times 8\ [cm]$) with various shapes. The overall comparison between those different structures under the same wind inlet velocity is shown in Fig. 23. It can be seen from the Fig. 26 that the (1), (4), (5), (7), (10) flexible structures generated a significant enhancement in the heat transfer coefficient in the initial tests under the same wind inlet velocity and power inputs. The plot comparing the most significantly h and ΔT are shown in the plot of Fig. 24. It was calculated that the ΔT decreased by 26.6% and the heat transfer coefficient increased by 36% with the Flexible Structure (1), rectangular textile sheets with the dimension of 0.14[m] in length and 0.08[m] in width, for the most significantly enhanced case among the initial approach on effects of different shapes.

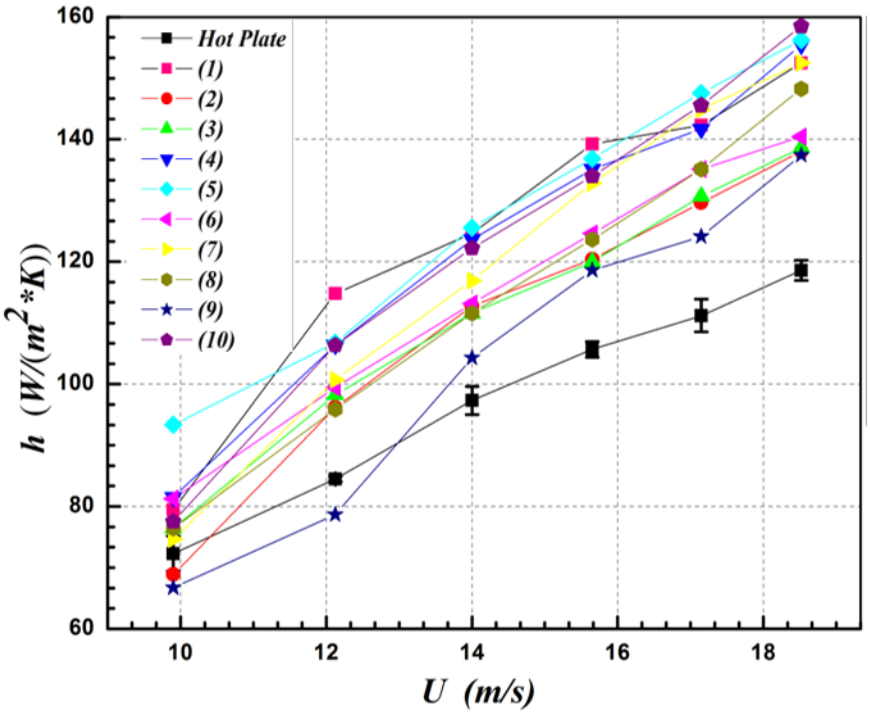

Figure 23 HTC experimental results with different shape of flexible structures

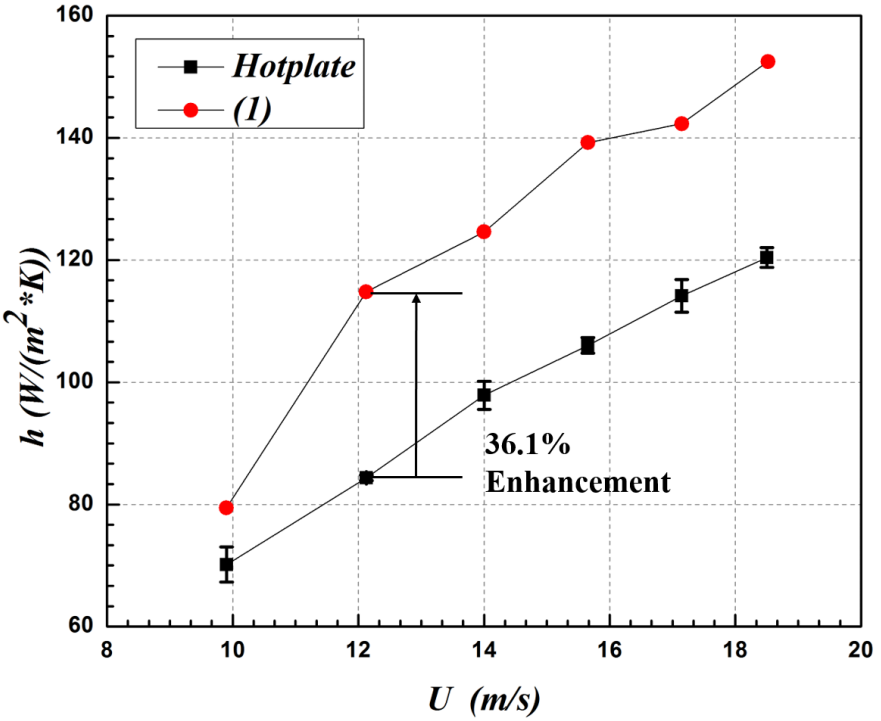

Figure 24 Most significant enhancement among different shape testing

Structures (1), (6), (8), (9), (10) were compared using the textiles with the same area, which is $0.0112\ [\mathrm{m}^2]$. The structures with equivalent areas include the following shapes: rectangular shape ($width$: $0.08\ [m]$; $length$: $0.14\ [m]$); Triangular shape ($Triangle\ Bottom$: 0.16 [m]; $Height$: $0.14[cm]$, placed in 2 directions); Trapezoid shape (Top: 4 [cm]; Bottom: 12 [cm]; and height 14 [cm], placed under 2 different directions). Fig. 25 indicates the performance of heat transfer coefficient for those 5 different shapes under different orientations.

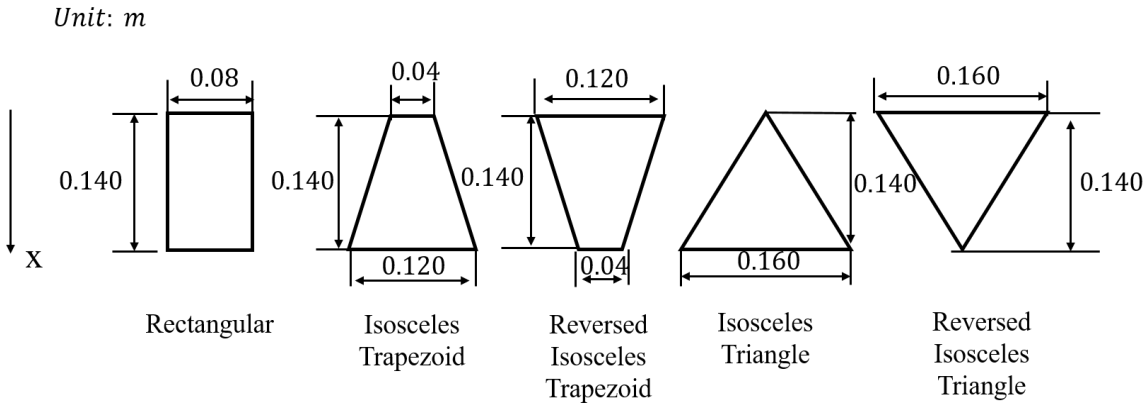

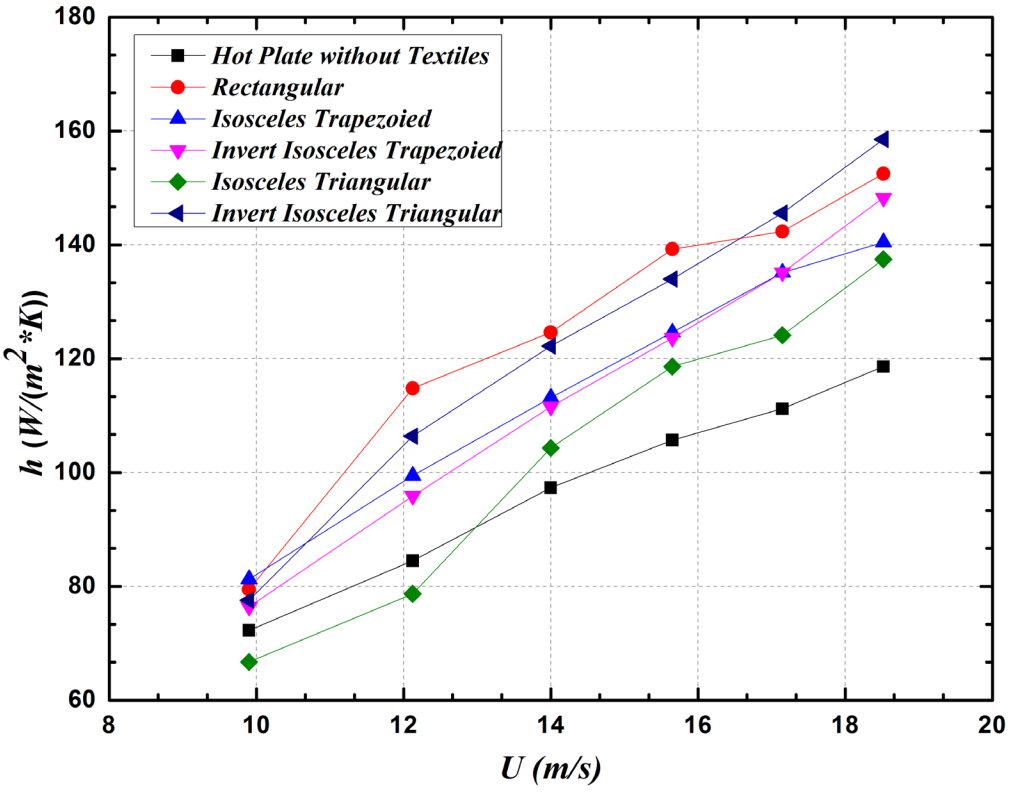

Figure 25 HTC performances with different shapes with fixed A_t

As shown in Fig. 25, under the same coverage area, the rectangular and the invert triangular textiles always achieved higher air-side HTC at the hotplate through all the selected wind inlet velocity conditions except $U_\infty = 9.9\, m/s$. The averaged

HTC for original hotplate case located at a range from $72.3\ W/(m^2 * K)$ to $118.6\ W/(m^2 * K)$ at the wind inlet velocity from 9.9 m/s to 18.5 m/s. For the cases applied oscillating textiles, at $U_\infty = 12.1\ m/s$, the enhancement on HTC taken by the rectangular textile is around 36%, which is more significant than other shapes of textile. At $U_\infty = 14.0\ m/s$ and $15.7\ m/s$, the rectangular textile also resulted in the highest HTC, which reached $125\ W/(m^2 * K)$ and $139\ W/(m^2 * K)$, respectively. However, at $U_\infty = 17.1\ m/s$ and $U_\infty = 18.5\ m/s$, the invert isosceles triangular shape has the highest HTC, which approached $145.6\ W/(m^2 * K)$ and $158.2\ W/(m^2 * K)$, respectively.

In the meantime, considering plotted the HTC performance as a function of the ratio of the front edge dimension to back edge dimension under a certain textile area with the same textile length, it also indicated that when the ratio is 1, that is, with the rectangular shapes, the HTC performance reached the highest enhancements under most wind velocity inlets.

(1), (3), (4) and (5) are the rectangular shape textiles approached at the initial stage with different dimensions. An initial hypothesis about controlling the width or length of the flexible textiles were conducted, and the experimental HTC performances are shown in the following Fig. 26.

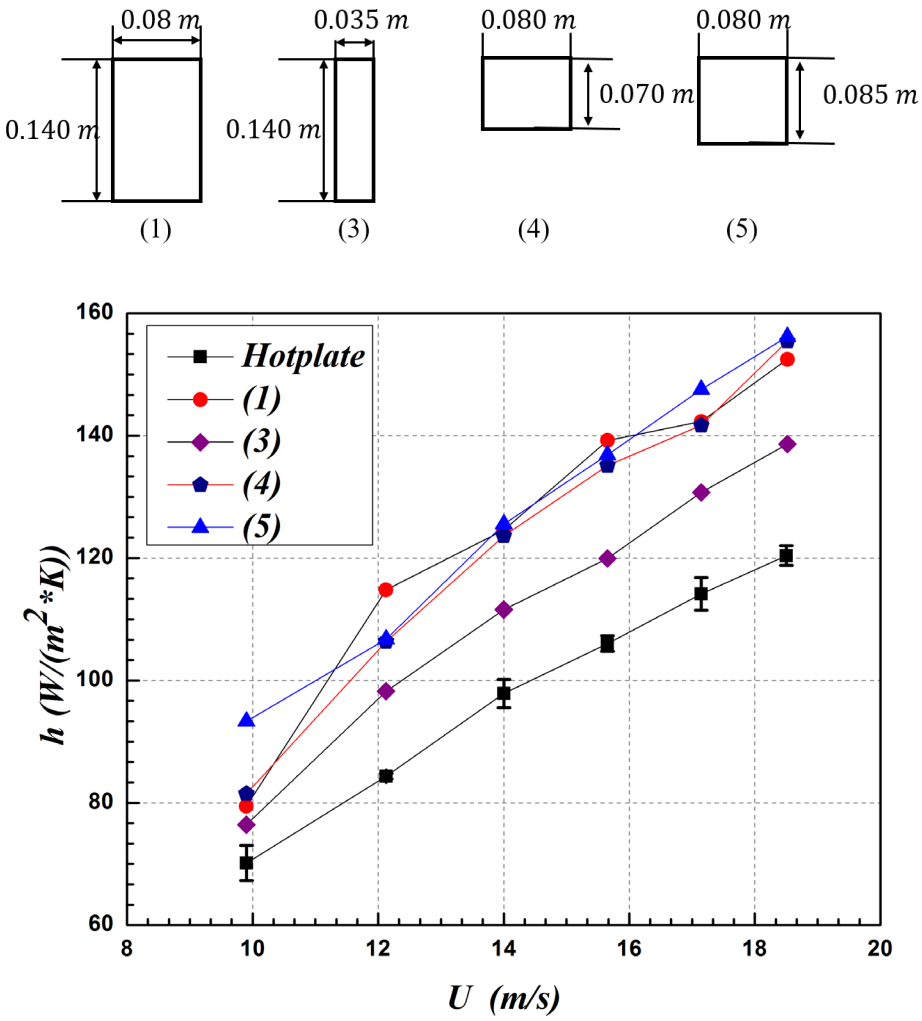

Figure 26 HTC results based on initial dimensional hypothesis

Fig. 27 compares the heat transfer performance under controlled width among those selected with rectangular dimensions. Comparing the experimental results for controlled length of flexible textiles, it seems that the width dimension could have large effects on the corresponding HTC performances.

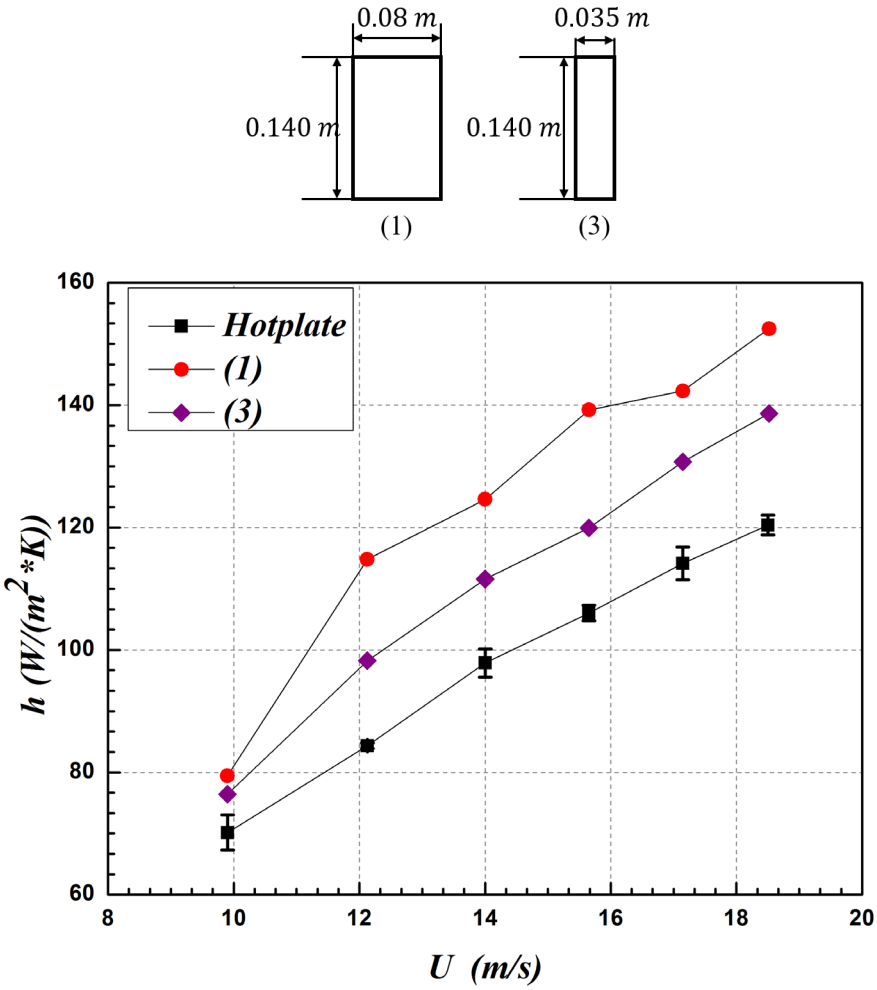

Figure 27 HTC performance controlled L (0.14 m) with W in (1) 0.08 m; (3) 0.035 m

Based on the experimental results above, the discussion regarding the dimensions of textile and their corresponding impact on heat transfer performance was raised, which will be futherly discussed in chapter 6. The dynamic properties observed through high-speed camera and its relationship between it and heat transfer performance will also be discussed in chapter 6.

Chapter 6: Effects of Dimensional Parameters and Oscillation Frequencies for Rectangular Textiles

6.1 Textile Design:

The following experiments are designed using selected rectangular-shape textiles to investigate their dimensional effects on the heat transfer coefficients. Taking the complete dimension of hot plate as the dimension scale, the lengths of the textiles were selected to be 30% (i.e. 0.045 [m]), 50% (i.e. 0.075 [m]), 80% (i.e. 0.120 [m]) and 100% (i.e. 0.150 [m]) of length of the hotplate. Similarly, the widths of the textiles were selected to be 50% (i.e. 0.635 [m]), 80% (i.e. 101.6 [mm]) and 100% (i.e. 0.127 [m]) of the width of the hotplate. Fig. 28 indicates the design of various rectangular shapes of the flexible structures, and all dimensional combinations were selected.

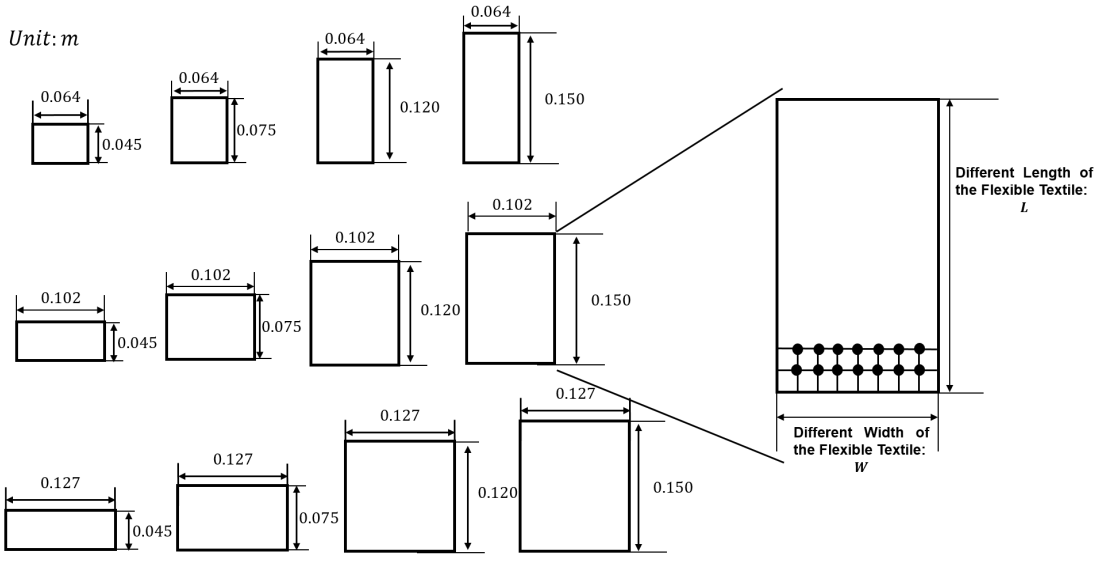

Figure 28 Schematic of selected shapes of rectangular textiles with meshes

6.2 Thermal Experiments

A total number of 72 sets of the convective heat transfer experiments were conducted to investigate the dimensional effects of the different flexible rectangular textile structures.

In this stage, the wind inlet velocity was the controlling parameter. Based on different wind inlet velocities, the scatter plot of heat transfer coefficients as a function of inlet wind velocity related to the dimension of flexible structures are shown in Fig. 29. Two independent studies were then conducted to compare the soft oscillating flexible microfiber structure with different lengths and the same width as well as the soft oscillating flexible microfiber structure under different width scale with the same length. Those comparisons are plotted in Fig. 30 and Fig. 31.

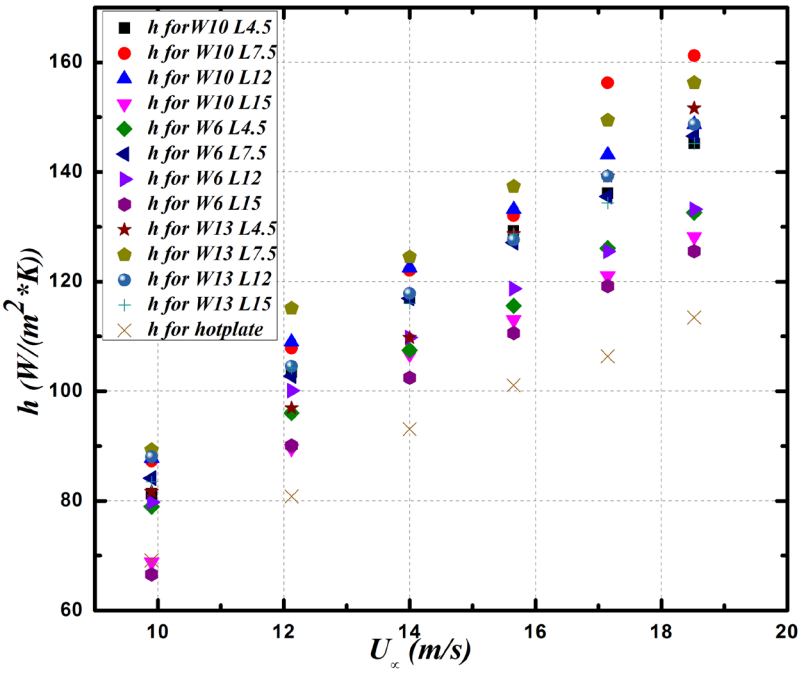

Figure 29 Scatter for HTC performance of different dimensions of rectangular structures. Legend in unit: cm

As can be seen in Fig. 30, with the same upstream wind velocity inlet, the flexible structures with length equal to half of the length of the heated plate provided the highest enhancement in heat transfer coefficient regardless of the width. In terms of the width effects, Fig. 31 shows that the flexible structure covering 80% and 100% of the hotplate width could provide the best heat transfer performance if the length of the flexible structures are the same, which is consistent with the result from the previous chapter (i.e. wider textiles could provide better HTC performances).

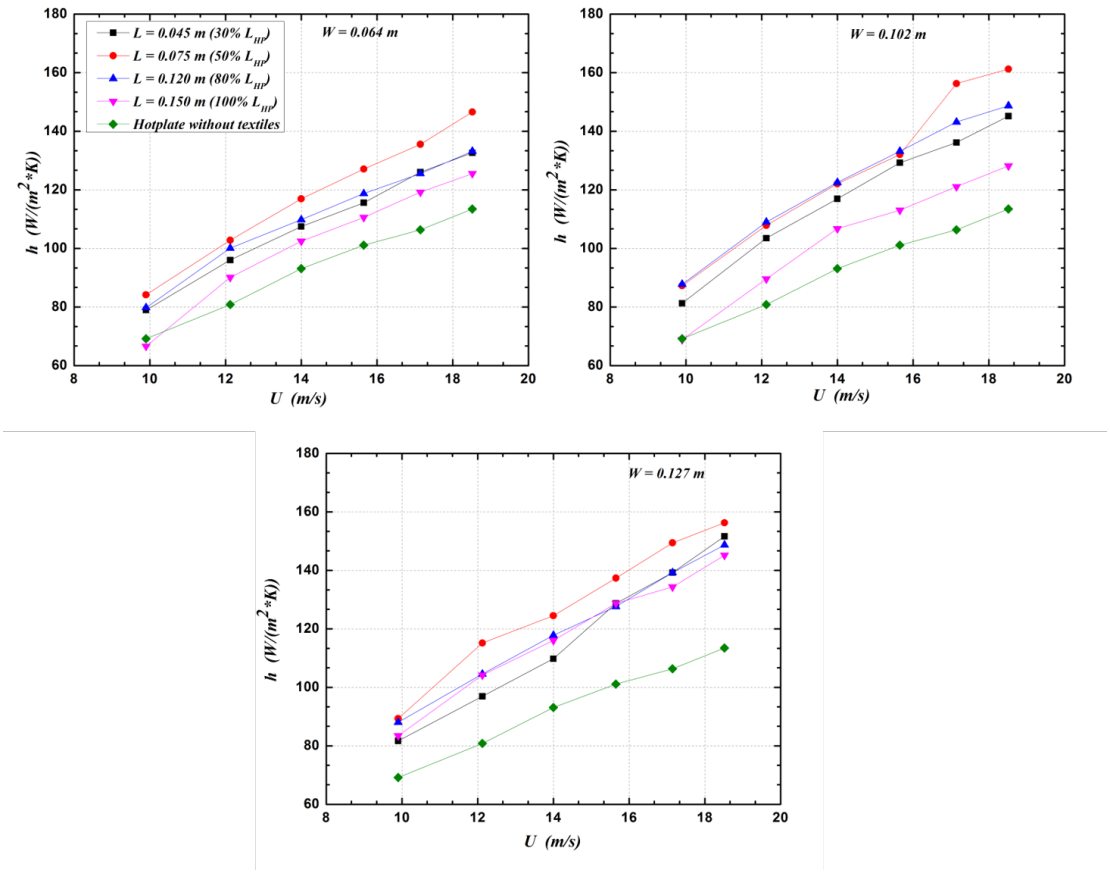

Figure 30 HTC in respect of U (Fixed W)

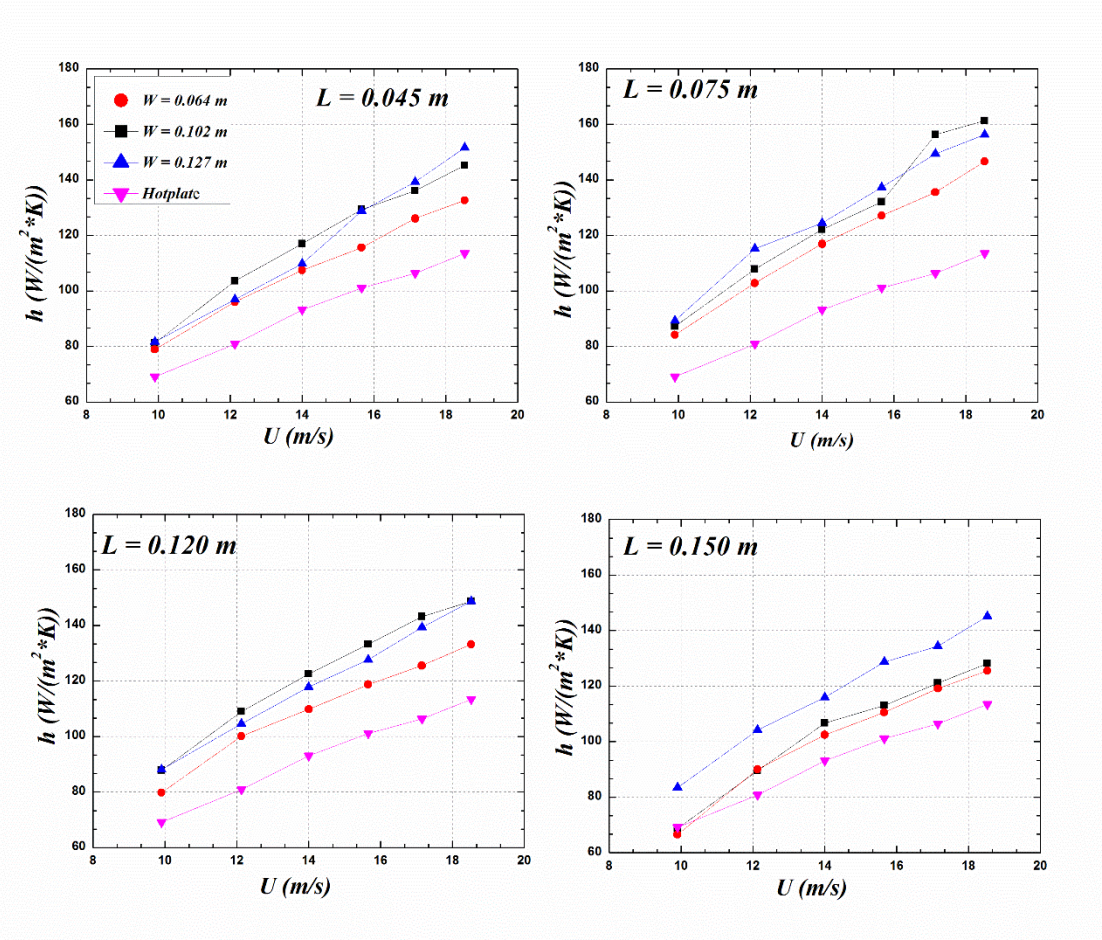

Figure 31 HTC in respect of U (Fixed L)

Fig. 32 compared the heat transfer coefficients for those textiles with the same width, in respect to their length. The figures show that the trends of heat transfer coefficient did not always increase with the length of the rectangular textile sheets. Actually, the maximum heat transfer coefficient always happens in the cases when the length of the flexible rectangular textiles reached half of the length of the hotplate.

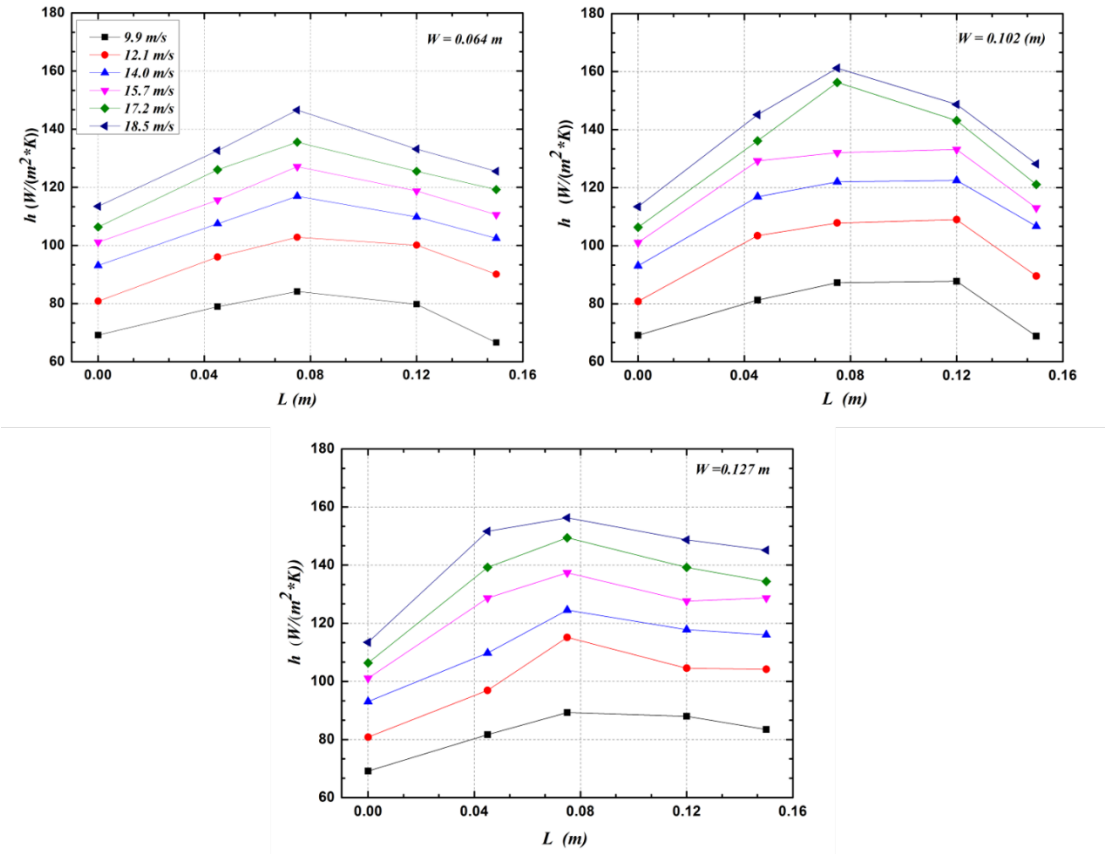

Figure 32 Effect of length on heat transfer performance

The length of the flexible textile could have an impact on its dynamic oscillating features and the textile affected area, which might also be related to the turbulent level of the fluid field inside the wind tunnel as well as the mixing level of core flow and the heated flow. To further investigate the joint effects of textile dimension and textiles' oscillating features, the following section focused on the observation of dynamic properties of those oscillating structures through the high-speed camera.

In the meantime, it was found that the largest heat transfer enhancement happened under the textile dimension of $0.075\ [\mathrm{m}] \times 0.102[\mathrm{m}]$ at the airflow inlet velocity of $17.15\ [\mathrm{m/s}]$. In this situation, the average heat transfer coefficient reached $156.28[\mathrm{W/(m^2 * K)}]$ from the original hot plate case of $113.14\ [\mathrm{W/(m^2 * K)}]$. All of

those rectangular textiles have a positive effect on the HTC performance, even the relatively thin or short cases. For example, with the textile dimension of 0.064 [m] $\times$ 0.045[m] under the wind inlet velocity of 12.12 $[m/s]$, the $h_{average}$ increased to 96.02 $[W/(m^2 * K)]$ compared to original hotplate case at 84.36 $[W/(m^2 * K)]$.

6.3 Effect of Oscillating Frequency

As previously mentioned, it is also important to study the relationship between the heat transfer performance and the oscillating frequency of the flexible structures. As shown in Fig. 32, for a better observation, several meshes and dots were drawn on the rectangular textile sheet, which made it easier to track the movement. In the following section, all dimensional combinations of rectangular textiles were observed and captured through high-speed cameras, and their oscillating cycles are determined by tracking time length taken for the highlighted dots to return to the same 2D position in the recording.

6.3.1 Stable Oscillation under Different Wind Inlet Velocities

A relatively stable and periodic oscillation could be found at most of the dimensional combinations of rectangular textiles. The following Fig. 33 to Fig. 35 show the typical oscillating periods using the rectangular textile dimension combination of 0.075 $[m]$ in length and 0.102 $[m]$ in width, 0.075 $[m]$ in length and 0.064 $[m]$ in width, and 0.075 $[m]$ in length and 0.045 $[m]$ in width. At the wind inlet velocity of 18 $[m/s]$, the oscillating frequencies range between 55 Hz to 77 Hz. The figure sets below are captured at a time step for every 0.003 $[s]$ for at least one completed oscillating time period.

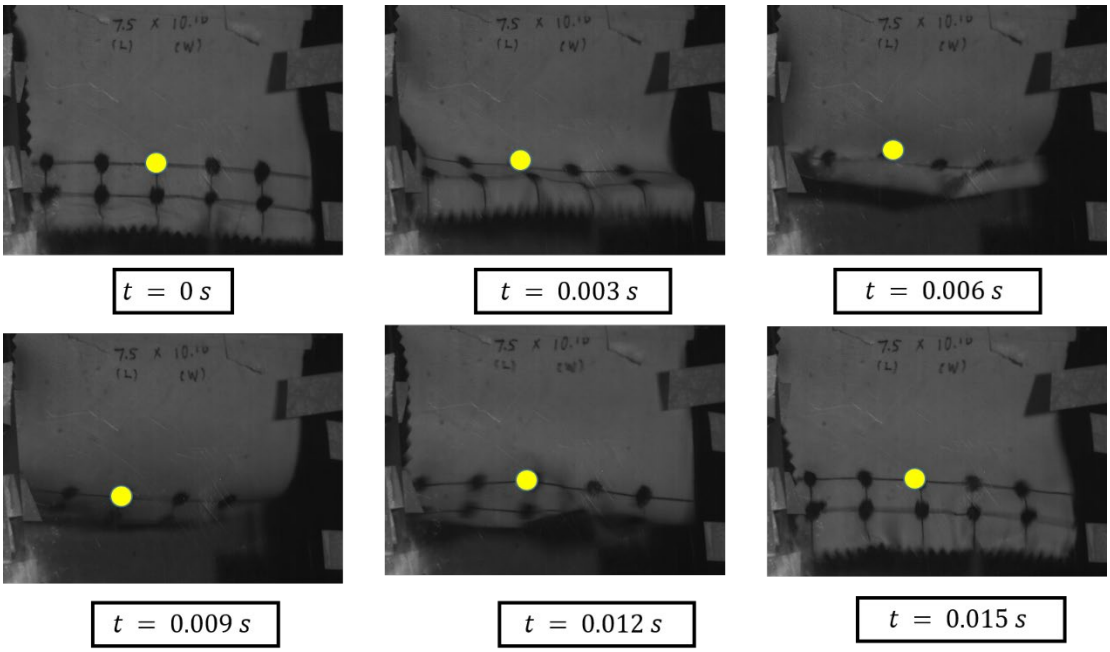

Figure 33 Oscillating dynamic observation for rectangular textile (L × W: 0.075 [m] × 0.102[m]; $f = 66.67\ Hz$ (T ≅ 0.015 [s]) , highlighted dot is used for tracking its dynamic traces.)

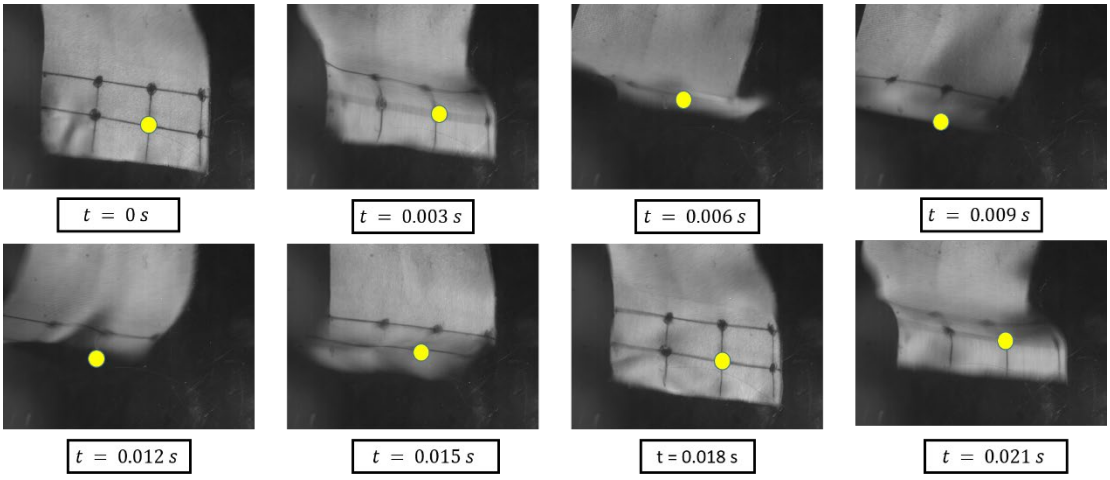

Figure 34 Oscillating dynamic observation for rectangular textile (L × W: 0.075 [m] × 0.064[m]; $f = 55.56\ Hz$ (T ≅ 0.018 [s]), highlighted dot is used for tracking the traces)

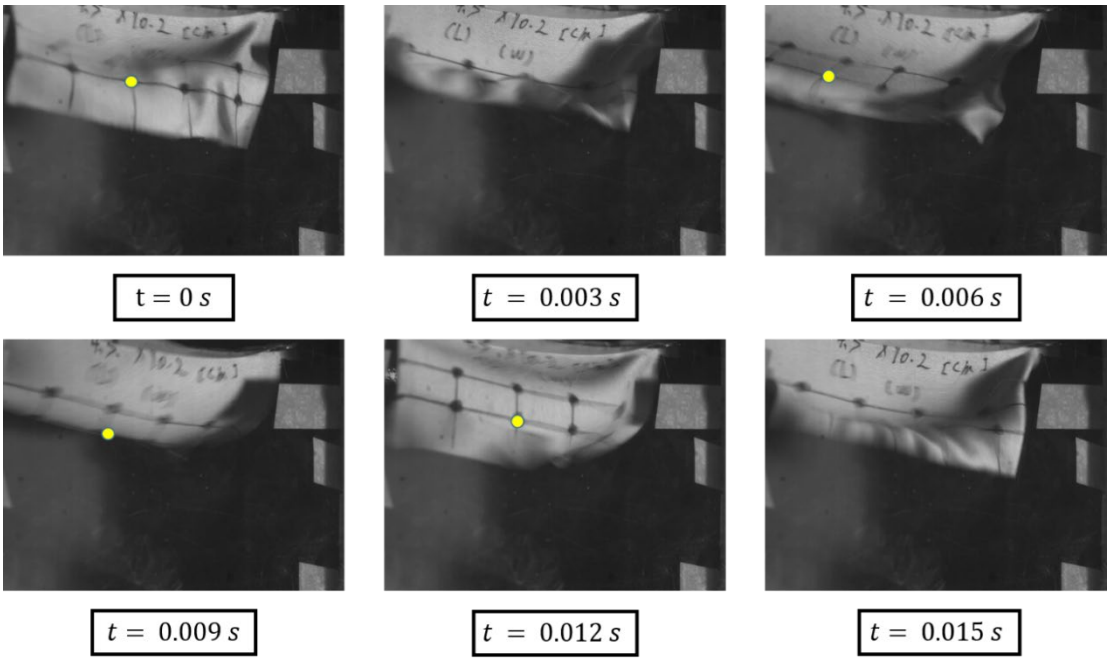

Figure 35 Oscillating dynamic observation for rectangular textile (L × W: 0.075 [m] × 0.044[m]; $f = 76.92\ Hz$ (T ≅ 0.018 [s]), Highlighted dot is used for tracking the traces)

By comparing Fig. 33 and Fig. 34, the observation shows that, as the width decreases from 0.102 m to 0.064 m, the corresponding frequency significantly decreased. Also, comparing Fig. 33 and Fig. 34, the observation show that, as the length decreases from 0.075 m to 0.045 m, the corresponding frequency significantly increased.

From the observations that the oscillating periods could be clearly counted and calculated, a negative relationship between the structure length and the oscillating frequency was observed, which is consistent with the observations from Fig. 33 to Fig. 35. Fig. 36 shows the scatter of oscillating frequency in respect of the textile length.

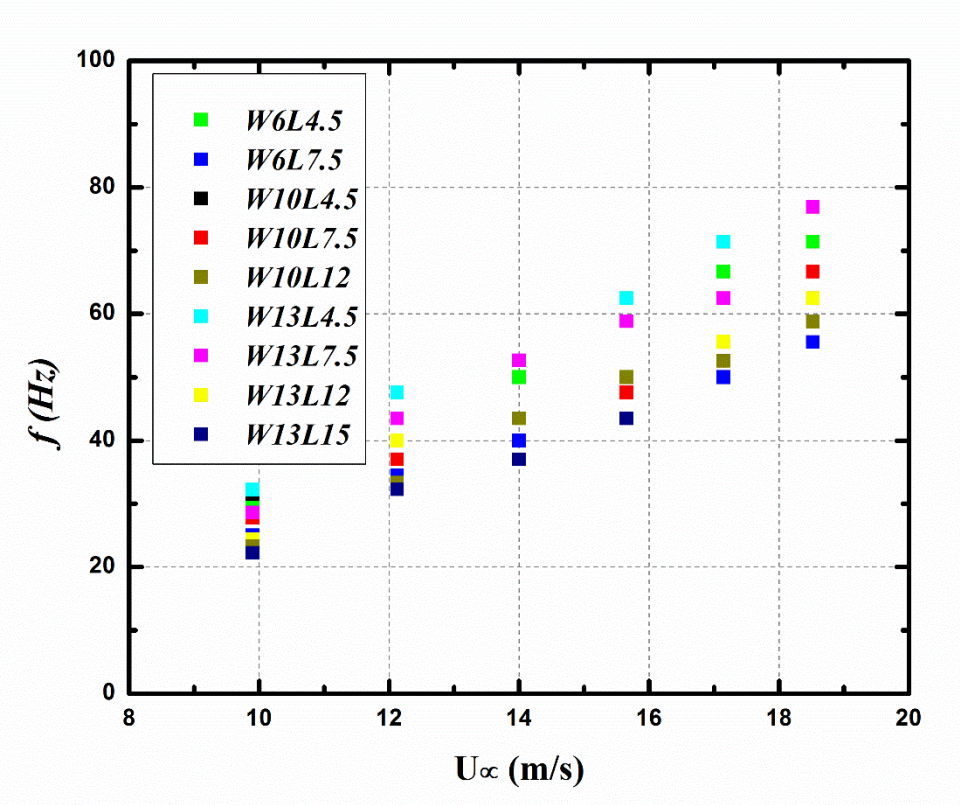

Figure 36 Oscillating frequency f in respect of inlet wind velocity U_{∞}. Legend in unit: cm

All of the oscillating frequency data are plotted in Fig. 36 above. The counted frequencies are in the upstream wind inlet velocity range of 9.9 m/s to 18 m/s, and the oscillating frequency calculated using the reverse of oscillating period was within the range approximately from 15.4 Hz to 76.9 Hz.

Table 8 contains all the oscillating frequency data collected, and it also shows that at some specific dimensions, unexpected dynamic motions were observed which are marked unsteady in the table. This kind of situation occurs in some of the cases that the length of the rectangular textiles reached 80% and 100% of the hotplate length, and it also tends to occur with thinner textiles. In the meantime, the wind velocity may also

play an important role in it. It seems the chances that unsteady oscillations occurred are larger at a higher wind inlet velocity.

Table 8 Oscillating frequency observed through high speed camera (with 6 different wind inlet velocities: from top to bottom small cells: 9.9 m/s; 12.1 m/s; 14.0 m/s; 15.7 m/s; 17.1 m/s; 18.5 m/s)

Length / Width	45 [mm]	75 [mm]	120 [mm]	150 [mm]
63.5 [mm]	29.4	25	Unsteady	Unsteady
	43.5	34.5	Unsteady	Unsteady
	50.0	40.0	Unsteady	Unsteady
	62.5	43.5	Unsteady	Unsteady
	66.7	50	Unsteady	Unsteady
	71.4	55.6	Unsteady	Unsteady
101.6 [mm]	31.2	27.8	23.3	Unsteady
	43.5	37.0	33.3	Unsteady
	50.0	43.5	43.5	Unsteady
	58.8	47.6	50.0	Unsteady
	66.7	55.5	52.6	Unsteady
	76.9	66.7	58.8	Unsteady
127 [mm]	32.3	28.6	24.4	22.2
	47.6	43.5	40.0	32.3
	52.6	52.6	43.5	37.0
	62.5	58.8	50.0	43.5
	71.4	62.5	55.6	Unsteady
	76.9	76.9	62.5	Unsteady

In addition to the single-dimensional effect of textile geometry on the oscillating motion, the area of textiles had a two-dimensional effect, which resulted from the integral influences of length and width. Fig. 37 plots the oscillating frequencies and the corresponding polynomial fitting curves at the fixed inlet wind velocities, with respect to the area ratio A^*, which can indicate the relationship between them. In Fig. 37, the polynomial fitting results are based on the maximum error of 22%.

Fig. 37 also illustrates that with an increasing of the area of textile, the oscillating frequency decreased at each inlet wind velocity; this phenomenon is partially different from the result shown in Table 1. This difference shows that the influence of the length of textiles on oscillating frequency is greater than the influence of the overall dimension.

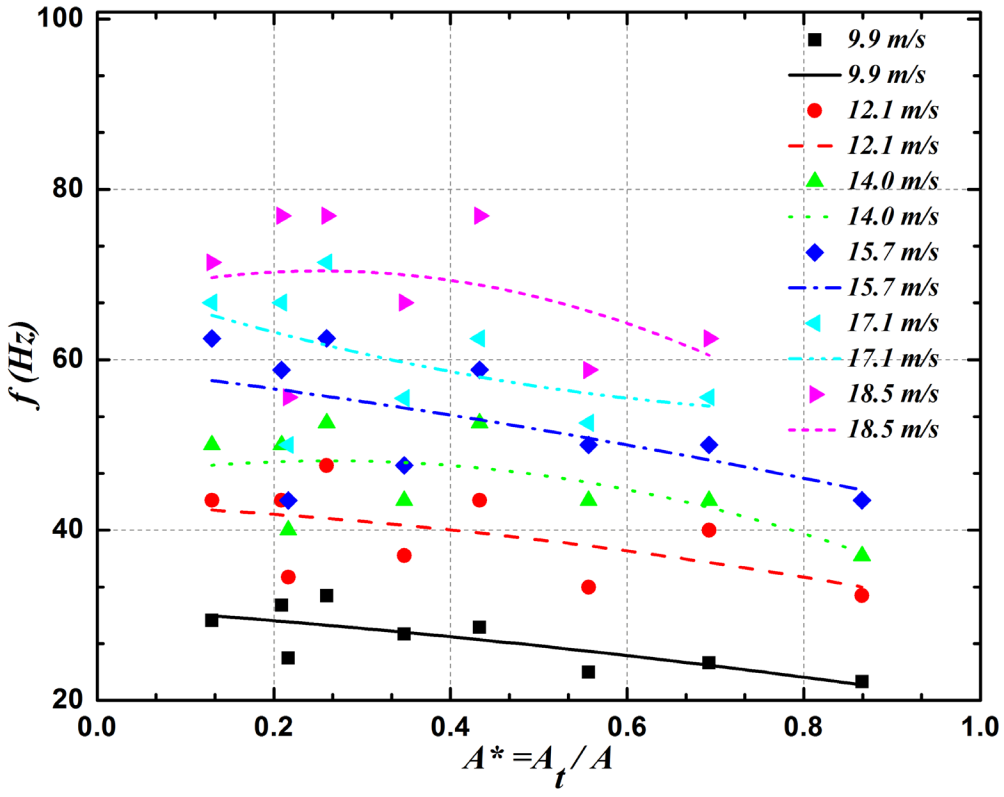

Figure 37 Oscillating frequency f in respect of textile area coverage ratio A^*

6.3.2 Unexpected Dynamic Motions at Irregular Regimes

As mentioned in the last section, it is also observed that the oscillation becomes unstable and irregular with the decreasing width and increasing length, which means it becomes more difficult to predict and analyze the flow field conditions and oscillating frequency. In Table 8, the motions with unsteady labels mean that the marked dots could not be continuously observed in the high-speed camera periodically, or the dynamic motion changed from regularly flapping to irregular swinging. In Fig. 38, two typical phenomena, (a).swinging and (b).sticking to the wall, are captured.

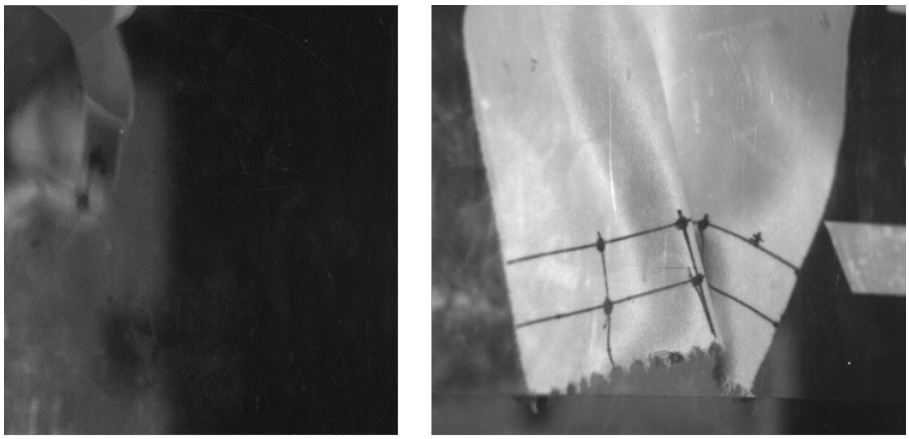

(a) (b)

Figure 38 Typical phenomena during irregular oscillations

((a). $L \times W$: 0. 150 × 0.064 m and (b). $L \times W$: 0.150 × 0.102m)

As shown in Fig. 38 (a), the textiles seemed to swing inside the channel, which did not show periodic oscillating or flapping features, and it did not touch and have effective influences on the hotplate boundary either. Oppositely, in Fig. 38 (b), the textile seemed to stick on the channel wall, which did not generate effective oscillations either. The unexpected motions found during the dynamic observation leads to a larger uncertainty in the frequency, which may affect the corresponding HTC performances.

The following Fig. 39 and Fig. 40 shows the captures of the two phenomena mentioned in a recording time of 90 s for a complete demonstration. Their effects on heat transfer performances will be discussed in the following sections. From Fig. 39, it seems difficult to continuously checking one dot on the mesh, and there seemed to be no method to effectively count the oscillation frequency. However, in Fig. 40, the time that the oscillating structure stuck to the wall is randomly distributed, which also results in the difficulties in counting and calculating the oscillating frequencies.

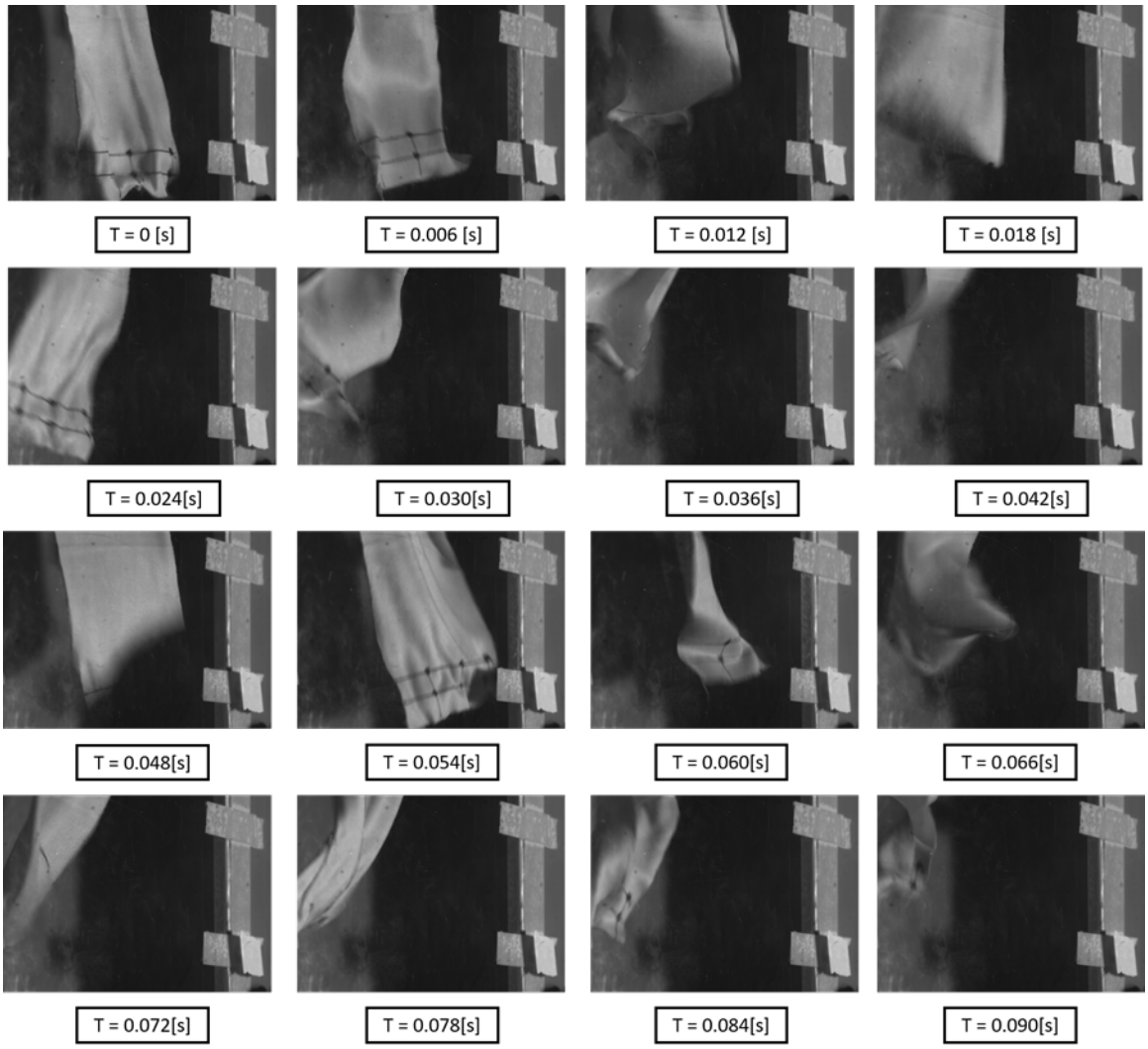

Figure 39 Irregular oscillating dynamic observation for rectangular textile

($L \times W$: 0.150 $m \times$ 0.064 m; $\mathrm{T}_{\mathrm{record}} =$ 0.090 s)

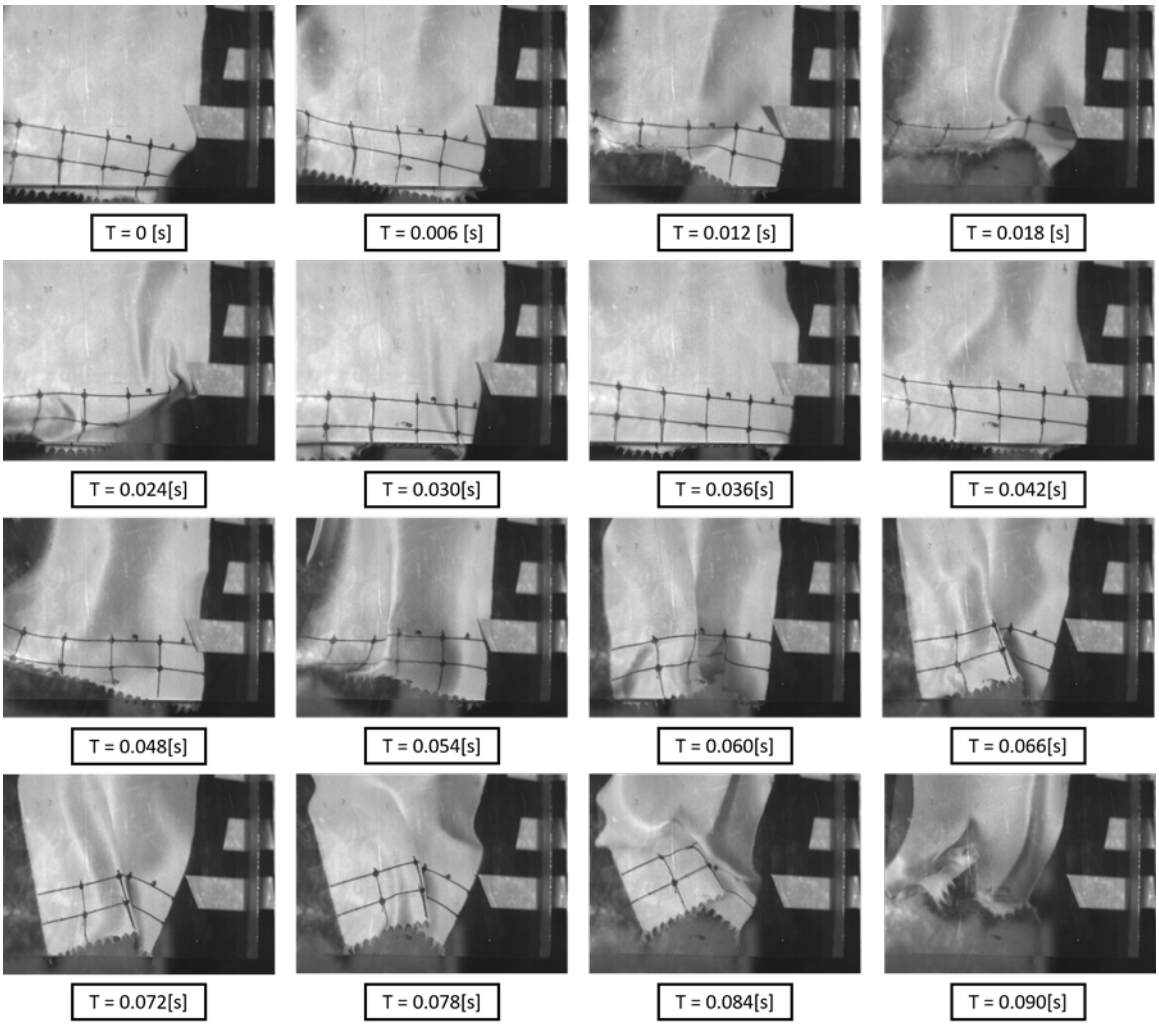

Figure 40 Irregular oscillating dynamic observation for rectangular textile

$$(L \times W: 0.150\ m \times 0.102\ m; T_{record} = 0.090\ s)$$

In the meantime, compared to other dimensions, it seems the dimensions that resulted in irregular oscillations always result in lower heat transfer performances (e.g. Length $\times$ Width: 0.120×0.064 [m]; 0.150×0.064 [m]; and 0.150×0.102 [m]). This phenomenon could also be explained through high-speed camera observations in section 6.3.

It could be observed in Fig.39 that the dynamic properties changed from flapping to random swinging when the width of the textile is only 50% of the heat

transfer area width. It could also be observed that the distance between the textile and the surface is unstable, and the textiles did not touch the surface for most of the time. This kind of irregular motions did not effectively disrupt the boundary layer development on the hot plate surface, which showed a lower heat transfer performance.

In Fig. 40, irregular motions seemed to be different than the previous case. During 0.090 [s] period of capture, it seems that nearly one-third of the time the textile was stuck to the wall. By doing that, it did not effectively mix the core flow and the near-surface boundary flow. Instead, since the thermal conductivity of the textile material is much lower than the aluminum, the textile acted like a thermally resistant layer when sticking to the hot plate surface, which would even reduce the heat transferring from the surface to the airflow.

6.4 Dimensionless Analysis

In this experimental study, the enhanced heat transfer performance by unsteady flow was achieved by 1) mixing the high-temperature boundary flow with low-temperature core flow and 2) disruption of the boundary layer.

Both the dimensional parameters and the oscillating features of the textiles could have influences on the two cases mentioned above. The dynamic oscillating properties could be analyzed from two aspects: the frequency of textile oscillating; and the displacement during the oscillating. However, due to the experimental equipment limitations, the displacement of those rectangular textiles cannot be determined. So, in this study, only the oscillating frequency was selected as the first parameter for analysis.

Additionally, the dimensional properties of those textiles could also affect the dynamic oscillating frequencies and the conditions of the fluid field, which means the area of rectangular textiles would jointly impact on the heat transfer performance. Therefore, the coverage ratio of rectangular textiles is selected as the second parameter for the investigation of impacts on heat transfer performances.

However, the dimensions of the rectangular textiles also have an impact on their corresponding oscillating frequency. Under the same wind velocity inlet, different dimensions of textiles could have large differences in their oscillating frequencies. Therefore, another dimensionless parameter that includes both the oscillating frequency of textiles and their dimensional parameters should be introduced. In this experimental study, the flow-induced oscillation frequency, f^* is introduced for overall analysis. The detailed f^* data calculated are presented in the following Table 9.

Table 9 Flow-induced oscillation frequency calculated for each rectangular dimension(with 6 different wind inlet velocities: From top to bottom small cells: 9.9 m/s; 12.1 m/s; 14.0 m/s; 15.7 m/s; 17.1 m/s; 18.5 m/s)

Length / Width	45 [mm]	75 [mm]	120 [mm]	150 [mm]
63.5 [mm]	0.133636364	0.189393939	Unsteady	Unsteady
	0.16177686	0.213842975	Unsteady	Unsteady
	0.160714286	0.214285714	Unsteady	Unsteady
	0.179140127	0.207802548	Unsteady	Unsteady
	0.175526316	0.219298246	Unsteady	Unsteady
	0.187894737	0.243859649	Unsteady	Unsteady
101.6 [mm]	0.141818	0.210606	0.282424	Unsteady
	0.16177686	0.229338843	0.330247934	Unsteady
	0.160714286	0.233035714	0.372857143	Unsteady
	0.168535032	0.227388535	0.382165605	Unsteady
	0.175526316	0.243421053	0.369122807	Unsteady
	0.202368421	0.29254386	0.412631579	Unsteady
127 [mm]	0.146818182	0.216666667	0.295757576	0.336363636
	0.177024793	0.269628099	0.396694215	0.400413223
	0.169071429	0.281785714	0.372857143	0.396428571
	0.179140127	0.28089172	0.382165605	0.415605096
	0.187894737	0.274122807	0.390175439	Unsteady
	0.202368421	0.202368421	0.202368421	Unsteady

From the experimental results in the previous sections, it was found that the trend of HTC performance is not always positively related to the oscillating frequencies if the dimensions of the textiles are also changed. As mentioned in previous paragraphs, the oscillating frequency decreases with increased length of textiles when the width of textiles is fixed. However, for the fixed width and wind velocity, the HTC increases with the $L_{textile}$ when $L_{\text{textile}} < 0.5L_{hotplate}$, but decreases with $L_{textile}$ when $L_{textile} > L_{hotplate}$. The higher oscillating frequency and larger coverage area would benefit the heat transfer performance, and the enhancement shown on heat transfer performance is a superimposed result that was affected by both parameters. When fixing the width of textiles, the increasing of length of the textiles could provide a larger effective area for the disruption inside the fluid domain. However, such a change also increased the resistance and the oscillating frequency correspondingly decreased. One possible explanation is that these two opposite length-based effects on heat transfer performances reach a balance point at around the length equal to 50% of the length of hot plate, and therefore the highest heat transfer coefficient happened in those cases.

Based on the Gnielinski correlation for turbulent channel flow [33], the Nusselt number for a certain wind inlet velocity and Reynolds number can be calculated. The Re_D reached 10^5 and f_D and Pr changed less than 7% in this study. Therefore, Nu can be simplified as $Nu = K \times (Re_D - 1000)$, where K can be considered as constants for given Reynolds number, which is actually a function of f_D and Pr.

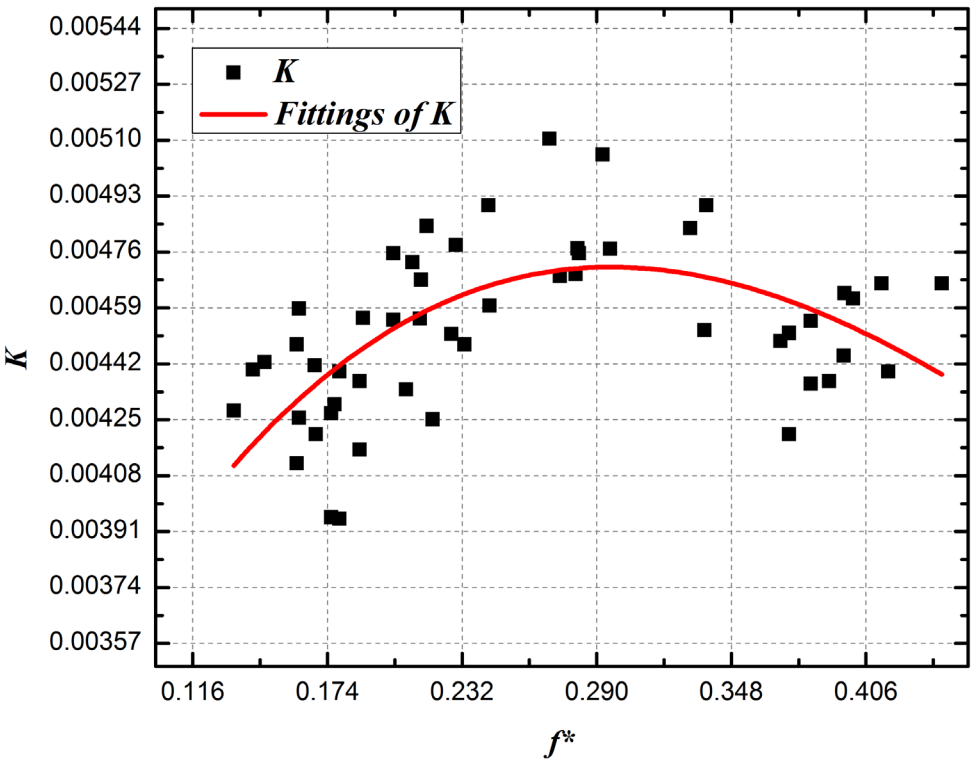

Figure 41 K related to the flow-induced oscillation frequency.

In Fig.41, the maximum value of K is achieved when f^* is in the range of 0.22 to 0.32. Therefore, for a given Reynolds number, the possible highest Nusselt number was achieved by optimizing the design of textile geometry to reach a flow-induced oscillation frequency in the range of $0.22\sim0.32$. This textile design provided an optimized convective heat transfer performance. Fig. 42 shows K highlighted in different colors, each representing different wind inlet velocities. The $K_{maximum}$ and its corresponding f^*slightly differed from each U_∞.

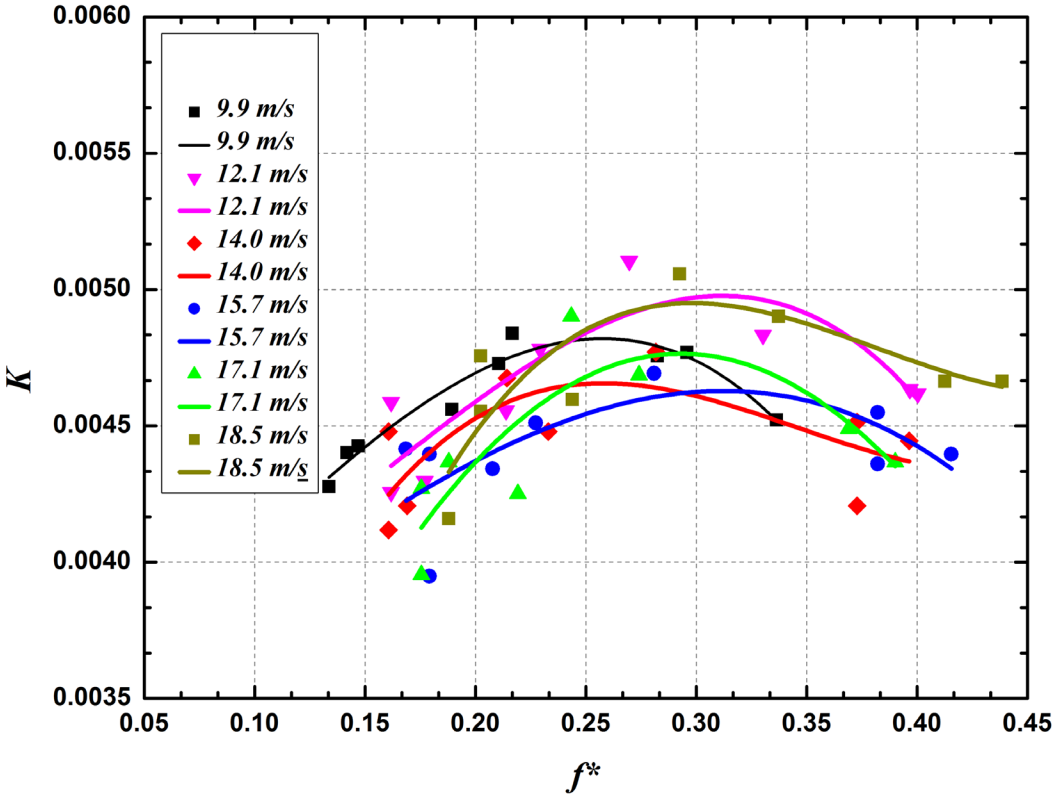

Figure 42 K related to the flow-induced oscillation frequency labeled by various colors.

The relationship between $A^*$and f^* is shown in Fig. 43. Each color represents one specific wind inlet velocity condition. It can be seen that f^* increased with the coverage ratio A* for a certain inlet wind velocity. In other words, an increase of fluid unsteadiness was found with an increase in coverage ratio. However, as shown in Figure 51, unsteadiness does not increase significantly when wind velocity is increased from 12.1m/s to 17.1m/s. Combining with Fig. 42, the possible area ratio for a given wind inlet velocity could be determined in order to achieve better heat transfer performance by maintain the flow-induced oscillation frequency $f^*{\sim}0.22-0.32$.

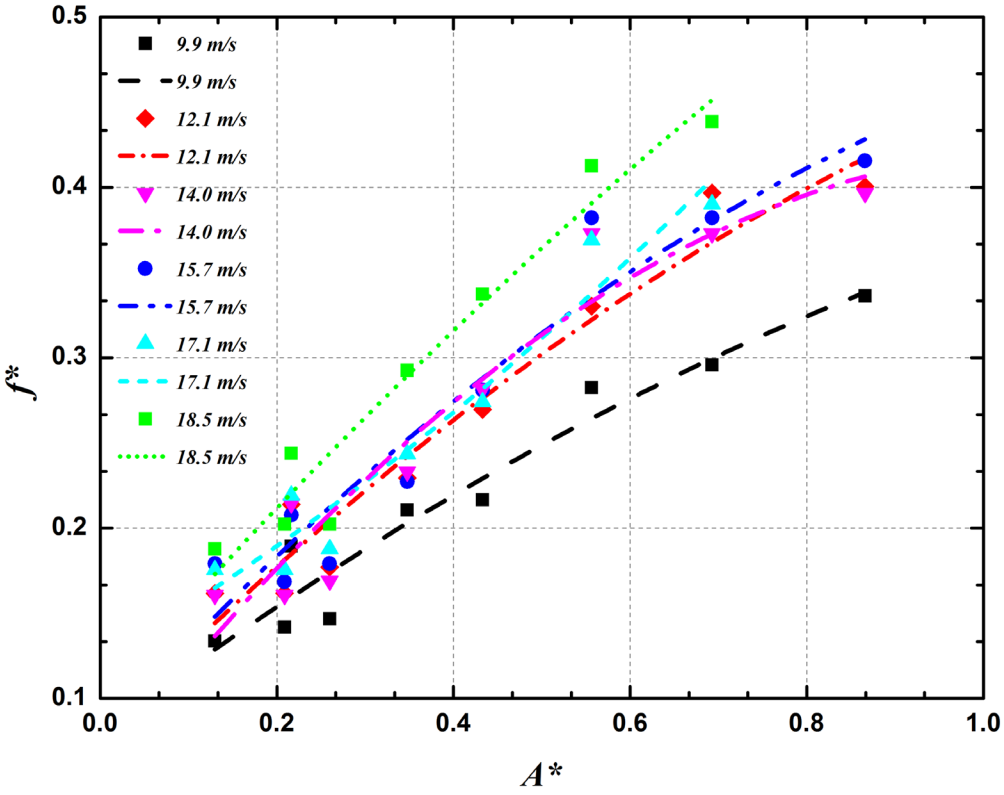

Figure 43 Flow-induced oscillation frequency in respect of textile area coverage ratio.

Chapter 7: Research Contributions and Conclusions

7.1 Research Contributions:

Although many uncertainties remain in this experimental study, the method for heat transfer enhancement by applying flow-induced flexible oscillating structures has been proven to be effective in most of the cases. With only one piece of rectangular shaped textile added onto the hotplate, the heat transfer coefficient could be improved by around 40% under the same inlet wind velocity. To the best of the author's knowledge, this study is not only one of the first experimental study in this research field, but also one of the first research studies focusing on both thermal and dynamic experiments for the effects of textile structures. Additionally, to my knowledge, most previous studies applying oscillating and vibrating structures were conducted in micro-channels or small dimension scale heat exchanges, while this experimental study, presented as part of the thesis research, applied this concept to a relatively large heat transfer area.

In addition, this experimental study could be useful for further materials exploration and parameter considerations for future experimental and industrial designs. Besides, the concept of applying textiles or other materials (i.e. soft, light, low-cost, and deformable, easy to fabricate and integrate into convective cooling applications) is also novel compared to existing cooling technologies, which means it may have significant potential for further developments and improvements.

7.2 Conclusions:

This thesis reports on an experimental heat transfer enhancement on a heated plate using a flow-induced oscillating flexible textile structure. The oscillation of textile flaps can enhance flow mixing and boundary layer disruption, and therefore increase the heat transfer between the hotplate and airflow. The heat transfer coefficient in the heated plate was measured for textile flaps with different sizes and shapes; the motion of the textile flap was captured using a high-speed camera.

Extensive experiments were conducted based on enhanced convective heat transfer conditions of a heated hot plate inside a vertical wind tunnel through adding low-cost passive flow-induced flexible structures. Preparations, correlations, and other experimental setups were done for this experimental study, and studies based on different parameters were also completed.

By comparing the effect of different shapes with the same coverage area, the rectangular shape was found to provide relatively better enhancement on heat transfer performance in most of the cases, which was represented by the experimental value of HTCs. Later on, the rectangular shape was selected for further dimensional analysis. The effects of dimensions (i.e. length and width of those rectangular textiles) are compared in respect of corresponding HTC enhancements. When the textile widths are fixed, the experimental results indicated that the maximum heat transfer performance often occurred when the length of those textiles is half of the hotplate length. The maximum heat transfer coefficient was found to be increased by around 40% in all cases.

Oscillating frequencies for different dimensional sets of those rectangular textiles were estimated using the high-speed camera. Based on high-speed camera observations, the shorter and wider textiles would result in faster oscillations and higher oscillating cycle frequencies. However, the textiles' oscillating features became unsteady with decreased width and increased length, which increased the uncertainty of the frequency estimation. To jointly consider the dimensional factors and dynamic oscillating influences, the effect of the overall textile coverage area and the dimensionless flow-induced oscillation frequency was analyzed. The heat transfer performances with respect to the flow-induced oscillation frequency f^* is represented by the coefficient $K = Nu/(Re - 1000)$ in this case. It was found the possible highest heat transfer performance was located in the range $0.22 \leq f^* \leq 0.32$. Correspondingly, a possible optimal design can be achieved by changing the area ratio for a certain inlet wind velocity to maintain a desired f^*.

Chapter 8: Recommendations for Future Work

Due to the current experimental facilities and existing limitations, this experimental study is still at its initial stage. Based on the previous approaches and the regulations founded, future work could be improved on both numerical analysis side and experimental side.

Firstly, the experimental setup design and assembly could be further improved. The current setup ignored the temperature differences through the hotplate and the heat loss through the conduction and radiation heat transfer. A more accurate improvement could, therefore, be made by using evenly distributed thermocouples to measure the temperatures across the entire heat transfer area, which could also obtain the temperature increment of the airflow after passing through the hotplate. Furthermore, Particle Image Visualization (PIV) could also be helpful for the fluid field experimental study, which can be used along with the high-speed camera applied to our previous approach. In the meantime, displacement sensors could be helpful for the displacement measurements of those flexible structures, which may contain further potential relationships between the HTC performances. Transparent wind tunnels that consist of acrylic sheets could also be helpful for high-speed camera observations from all directions, which may provide more information on textile flap tip displacements. Various kinds of soft materials could be further selected for the comparison between different stiffness, the mass ratio of materials and their corresponding effects on HTC performance.

Materials comparisons for further selection of flexible structures are needed, which needs to consider the temperature tolerance, the density, the stiffness, and the

cost of that specific kind of material. The mass ratio between the material of oscillating structure and the surrounding fluid can also impact the displacement of that structure, and the oscillating modes as well. Those material comparison with PIV flow visualizations can be beneficial for future researches regarding this topic. Further modifications and optimizations regarding the actual industrial applications of this technology is also needed. For example, in air to air heat exchangers, the solid structure design for textile placement and noise cancelling during the oscillating process need to be furtherly considered.

For the numerical analysis and CFD simulation, future works could focus on the Fluid-Structure Interaction (FSI), which requires dynamic mesh and sophisticated modeling. The modeling and simulation work for the unsteady flow disrupted by those flexible materials like textile could be difficult, especially in cases of unexpected dynamic motions. The three-dimensional numerical analysis and simulations may be necessary for those complicated fluid field predictions.

Bibliography

[1] S. Liu and M. Sakr, "A Comprehensive Review on Passive Heat Transfer Enhancements in Pipe Exchangers," *Renewable and Sustainable Energy Reviews*, vol. 19, pp. 64–81, 2013.

[2] M. Manno, B. Yang, and A. Bar-Cohen, "Near-junction "hot spot" suppression with integral SiC microcontact TEC," *International Journal of Heat and Mass Transfer*, vol. 115, pp. 530–536, 2017.

[3] Sumeer Khanna, Patrick McCluskey, Avram Bar-Cohen, Bao Yang, and Michael Ohadi, "Thin Thermally Efficient ICECool Defense Semiconductor Power Amplifiers." *Journal of Microelectronics and Electronic Packaging*, Vol. 14, pp. 77-93, 2017.

[4] O. Yemenici and H. Umur, "Experimental Aspects of Heat Transfer Enhancement over Various Flow Surfaces," *Heat Transfer Engineering*, vol. 37, no. 5, pp. 435–442, 2016.

[5] C. H. Li and G. P. Peterson, "Experimental Studies of Natural Convection Heat Transfer of Al 2 O 3 /DI Water Nanoparticle Suspensions (Nanofluids)," *Advances in Mechanical Engineering,* vol. 2, no. 4, p. 742739, 2010.

[6] S. Kakaç and A. Pramuanjaroenkij, "Review of Convective Heat Transfer Enhancement with Nanofluids*," International Journal of Heat and Mass Transfer*, vol. 52, no. 13-14, pp. 3187–3196, 2009.

[7] G. Li, Y. Zheng, G. Hu, Z. Zhang, and Y. Xu, “Experimental Study of the Heat Transfer Enhancement from a Circular Cylinder in Laminar Pulsating Cross-flows,” *Heat Transfer Engineering*, vol. 37, no. 6, pp. 535–544, 2016.

[8] E. I. Nesis, A. F. Shatalov, and N. P. Karmatskii, “Dependence of the Heat Transfer Coefficient on the Vibration Amplitude and Frequency of a Vertical Thin Heater,” *Journal of Engineering Physics and Thermophysics*, vol. 67, no. 1-2, pp. 696–698, 1995.

[9] A. Suksangpanomrung, S. Chungpaibulpatana, and P. Promvonge, “Numerical Investigation of Heat Transfer in Pulsating Flows Through a Bluff Plate,” *International Communications in Heat and Mass Transfer*, vol. 34, no. 7, pp. 829–837, 2007.

[10] J. Wajs, D. Mikielewicz, E. Fornalik-Wajs, and M. Bajor, “High Performance Tubular Heat Exchanger with Minijet Heat Transfer Enhancement,” *Heat Transfer Engineering*, vol. 37, pp. 1–12, 2018.

[11] P. Wang et al., “Sweating-boosted air cooling using nanoscale CuO wick structures,” *International Journal of Heat and Mass Transfer*, vol. 111, pp. 817–826, 2017.

[12] X. Wang, H. Hu, and X. Xu, “Photo-Acoustic Measurement of Thermal Conductivity of Thin Films and Bulk Materials,” *Journal of Heat Transfer*, vol. 123, no. 1, p. 138, 2001.

[13] X. Liu, A. Wang, S. Wang, and D. Dai, “Effects of wind on the dynamics of the central jet during drop impact onto a deep-water surface,” *Physical Review Fluids*, vol. 3, no. 5, 2018.

[14] X. Liu and J. H. Duncan, “The effects of surfactant on spilling breaking waves,” *Nature*, vol. 421, no. 6923, pp. 520–523, 2003.

[15] R. Webb, *Principles of Enhanced Heat Transfer*, Wiley-Interscience publication, John Wiley & Sons, 1994.

[16] C.-C. Wang, K.-Y. Chen, J.-S. Liaw, and C.-Y. Tseng, “An experimental study of the air-side performance of fin-and-tube heat exchangers having plain, louver, and semi-dimple vortex generator configuration,” *International Journal of Heat and Mass Transfer*, vol. 80, pp. 281–287, 2015.

[17] C.-C. Wang, “A survey of recent patents of fin-and-tube heat exchangers from 2001 to 2009,” *Int. Journal of Air-Conditioning and Refrigeration*, vol. 18, no. 01, pp. 1–13, 2010.

[18] A. M. Jacobi, R. K. Shah, “Heat Transfer Enhancement through the Use of Longitudinal Vortices: A Review of Recent Progress”, *Experimental Thermal and Fluid Science*, 11, pp. 295–309

[19] M. C. Gentry, A. M. Jacobi “Heat Transfer Enhancement by Delta-Wing-Generated Tip Vortices in Flat-Plate and Developing Channel Flows” *Journal of Heat Transfer*, Vol. 124, December 2002

[20] C.-C. Wang, K.-Y. Chen, “An experimental study of the air-side performance of fin-and-tube heat exchangers having plain, louver, and semi-dimple vortex generator configuration”, *International Journal of Heat and Mass Transfer* 80 (2015) 281–287

[21] S. Ali, et al. “Heat transfer and mixing enhancement by free elastic flaps oscillation.” *International Journal of Heat and Mass Transfer* 85, pp. 250–264. DOI: 10.1016/j.ijheatmasstransfer.2015.01.122.

[22] Z. Li et al., “Airfoil-shaped self-agitator for convective heat transfer enhancement,” *International Journal of Thermal Sciences*, vol. 133, pp. 284–298, 2018.

[23] T. Açıkalın, S. M. Wait, S. V. Garimella, and A. Raman, “Experimental Investigation of the Thermal Performance of Piezoelectric Fans,” *Heat Transfer Engineering*, vol. 25, no. 1, pp. 4–14, 2004.

[24] T. Açıkalın, S. V. GARIMELLA, A. RAMAN, and J. Petroski, “Characterization and optimization of the thermal performance of miniature piezoelectric fans”, *International Journal of Heat and Fluid Flow,* Volume 28, Issue 4, August 2007, Pages 806-820

[25] S. M. Wait, S. Basak, S. V. Garimella, and A. Raman, Eds., “Piezoelectric Fans Using Higher Flexural Modes for Electronics Cooling Applications IEEE Transactions on Components and Packaging Technologies, vol. 30 No.1 pp 119-128, 2007

[26] J. H. Yoo, J. I Hong, and W. Cao; “Piezoelectric ceramic bimorph coupled to thin metal plate as cooling fan for electronic devices;” *Sensors and Actuators* 79 2000 8–12

[27] D. Gerty, Fluidic-driven Cooling of Electronic Hardware Part I: Channel Integrated Vibrating Reed Part II: Active Heat Sink Ph.D. Thesis, 2008

[28] P. Hidalgo, F. Herrault, M. Allen, A. Glezer, S. Kaslusky and B. St. Rock, "Heat transfer enhancement in high-power heat sinks using active reed technology," *16th International Workshop on Thermal Investigations of ICs and Systems,* pp. 1-6, 2010.

[29] F. Herrault, P. Hidalgo, C. Ji, A. Glezer, and M. Allen, “Cooling performance of micromachined self-oscillating reed actuators in heat transfer channels with integrated diagnostics,” in *Micro Electro Mechanical Systems*, Proceedings of the IEEE 25th International Conference On Micro Electro Mechanical Systems (MEMS), Paris, France, 2012 (IEEE, 2010), pp. 1217–1220

[30] K. Shoele and R. Mittal, “Computational study of flow-induced vibration of a reed in a channel and effect on convective heat transfer,” *Physics of Fluids* 26, 127103 (2014)

[31] J. B. Lee, S. G. Park, and H. J. Sung, “Heat transfer enhancement by asymmetrically clamped flexible flags in a channel flow,” *International Journal of Heat and Mass Transfer*, vol. 116, pp. 1003–1015, 2018.

[32] Virot, Emmanuel; Amandolese, Xavier; Hémon, Pascal (2013): Fluttering flags: An experimental study of fluid forces. *Journal of Fluids and Structures* 43, pp. 385–401. DOI: 10.1016/j.jfluidstructs.2013.09.012.

[33] T. L. Bergman and F. P. Incropera, *Fundamentals of Heat and Mass Transfer*, 7th ed. Hoboken NJ: Wiley, 2011.

[34] J. Helton W. Oberkampf and K. Sentz. Mathematical representation of uncertainty, AIAA-paper 2001-1645. In 42th AIAA/ASME/ASCE/AHS/ASC Structures Dynamics, and Materials Conference and Exhibit, Seattle, WA, January 2001. CD-ROM.